NUREG/CR-2778
ANL-82-32

NUREG/CR-2[illegible]3
ANL-82-[illegible]2

CORRELATION FOR NUCLEATION SITE DENSITY AND ITS EFFECT ON INTERFACIAL AREA

by

G. Kocamustafaogullari, I. Y. Chen,
and M. Ishii

ARGONNE
NATIONAL
LABORATORY

ARGONNE NATIONAL LABORATORY, ARGONNE, ILLINOIS

Prepared for the Office of Nuclear Regulatory Research
U. S. NUCLEAR REGULATORY COMMISSION
under Interagency Agreement DOE 40-550-75

The facilities of Argonne National Laboratory are owned by the United States Government. Under the terms of a contract (W-31-109-Eng-38) among the U. S. Department of Energy, Argonne Universities Association and The University of Chicago, the University employs the staff and operates the Laboratory in accordance with policies and programs formulated, approved and reviewed by the Association.

MEMBERS OF ARGONNE UNIVERSITIES ASSOCIATION

The University of Arizona
Carnegie-Mellon University
Case Western Reserve University
The University of Chicago
University of Cincinnati
Illinois Institute of Technology
University of Illinois
Indiana University
The University of Iowa
Iowa State University
The University of Kansas
Kansas State University
Loyola University of Chicago
Marquette University
The University of Michigan
Michigan State University
University of Minnesota
University of Missouri
Northwestern University
University of Notre Dame
The Ohio State University
Ohio University
The Pennsylvania State University
Purdue University
Saint Louis University
Southern Illinois University
The University of Texas at Austin
Washington University
Wayne State University
The University of Wisconsin-Madison

Available from

GPO Sales Program
Division of Technical Information and Document Control
U. S. Nuclear Regulatory Commission
Washington, D.C. 20555

and

National Technical Information Service
Springfield, Virginia 22161

NUREG/CR-2778
ANL-82-32

(Distribution
Codes: R2
and R4)

ARGONNE NATIONAL LABORATORY
9700 South Cass Avenue
Argonne, Illinois 60439

CORRELATION FOR NUCLEATION SITE DENSITY AND ITS EFFECT ON INTERFACIAL AREA

by

G. Kocamustafaogullari,* I. Y. Chen,*
and M. Ishii

Reactor Analysis and Safety Division

May 1982

Prepared for the Division of Reactor Safety Research
Office of Nuclear Regulatory Research
U. S. Nuclear Regulatory Commission
Washington, D. C. 20555
Under Interagency Agreement DOE 40-550-75

NRC FIN No. A2026

*University of Wisconsin at Milwaukee

CORRELATION FOR NUCLEATION SITE DENSITY
AND ITS EFFECT ON INTERFACIAL AREA

by

G. Kocamustafaogullari, I. Y. Chen and M. Ishii

ABSTRACT

The bubble number density is important for the determination of interfacial area in boiling two-phase flow. The interfacial area is a key parameter affecting the interfacial transfer of mass, momentum and energy between phases. For a two-fluid model formulation of two-phase flow analyses, therefore, the bubble number density is quite important, however, there have been no correlations available to calculate this parameter. In view of this, a new correlation for the number density of the active wall nucleation site as well as the calculational method to obtain the bubble number density in boiling flow were developed here. The model was developed first for a pool boiling system and then it was extended to a forced convection system.

NRC
FIN No. | Title

A2026 | Phenomenological Modeling of Two-Phase Flow in Water Reactor Safety

TABLE OF CONTENTS

LIST OF FIGURES

LIST OF TABLES

NOMENCLATURE

NOMENCLATURE

A_c	Cross sectional area
A_b	Projected area of a particle
A_i	Surface area of a particle
a	Thermal diffusivity
a_i	Interfacial area concentration (interfacial area per unit volume)
B_b	Volume of a particle
C_p	Specific heat at constant pressure
D	Tube diameter
D_d	Bubble departure diameter
D_{dF}	Bubble departure diameter predicted by Fritz equation
F	Parameter defined by Eq. (76)
f	Bubble generation frequency
G	Mass velocity
g	Gravity
h	Heat transfer coefficient
i	Enthalpy
i_{fg}	Heat of evaporation
k	Thermal conductivity
N_a	Active nucleation site density in forced convective nucleate boiling
N_p	Active nucleation site density in pool boiling
N_b	Bubble number density
N^*	Dimensionless active nucleation site density defined as $N^* = ND_d^2$ where $N = N_a$ or N_p
Nu	Nusselt number
$\hat{n}$	Unit-vector normal to the channel wall directed away from the fluid
$\hat{n}_\xi$	Unit vector normal to ξ located in the cross sectional plane and directed away from the fluid

NOMENCLATURE (Cont'd)

P	Pressure
Pr	Prandtl number
$\dot{q}''$	Heat flux
R	Bubble radius
$\dot{R}$	Bubble growth velocity
R_c	Critical cavity size
R_{ce}	Critical cavity size based on effective liquid superheat
R_c^*	Dimensionless critical cavity radius defined as $R_c/(D_d/2)$
Re	Reynolds number
Re_{TP}	Two-phase flow Reynolds number defined by Eq. (74)
r	Radial coordinate in spherical coordinate system
r_D	Drag radius
r_d	Particle radius
r_s	Surface radius
r_{sm}	Souter mean radius
r_v	Equivalent radius (volume)
S	Suppression factor, defined by Eq. (73)
s	Average distance between neighboring active nucleation sites
T	Temperature
T_f	Bulk fluid temperature
T_o	Bulk fluid temperature at z_o
T_{sat}	Saturation temperature
T_w	Wall temperature
t	Time
v	Volume
$\vec{v}_b$	Local bubble velocity

NOMENCLATURE (Cont'd)

$\vec{v}_f$	Local liquid velocity associated with a growing bubble
$\bar{v}_f$	Characteristic mean liquid velocity associated with a growing bubble
$\vec{v}_\xi$	Channel wall velocity
X_{tt}	Martinelli parameter
x	Quality
z	Axial coordinate
z_o	Axial coordinate at point of incipient vapor formation
z_l	Axial coordinate at point $T_f = T_{sat}$
α	Void fraction
$\Delta\rho$	Mass density difference defined as $\Delta\rho \equiv \rho_f - \rho_g$
ΔT_{sat}	Wall superheat defined as $\Delta T_{sat} = T_w - T_{sat}$
η	Fraction of bubbles that re-condense, Eq. (23)
θ	Contact angle
μ	Dynamic viscosity
ν	Kinematic viscosity
ξ	Heated perimeter
ρ	Mass density
ρ^*	Nondimensional density difference, $\Delta\rho/\rho_g$
σ	Surface tension
ϕ	Bubble generation rate, defined as the number of bubbles generated per unit volume per unit time
ϕ_{he}	Heterogeneous bulk liquid nucleation rate
ϕ_{ho}	Homogeneous bulk liquid nucleation rate
ϕ_{si}	Bubble sink rate due to re-condensation
ϕ_{so}	Bubble source rate due to bulk liquid nucleation
ϕ_w	Bubble nucleation rate from active cavities

Subscripts

f	Liquid phase
g	Vapor phase
w	Wall

Superscripts

*	Dimensionless quantities

Averages

<< >>	Area average
< >	Line average

EXECUTIVE SUMMARY

The interfacial transfer terms in a two-fluid model formulation for two-phase flow analyses specify the rate of phase change, momentum exchange and heat transfer between phases. However, previous studies have indicated that the weakest link in the two-fluid model formulation is the constitutive relations for these interfacial terms. Unless these phase interaction terms are accurately modeled, the complicated model does not necessarily warrant accurate solutions.

It can be shown that the interfacial transfer terms are proportional to the interfacial area and driving force. Therefore, the first order geometrical effect of the interface on the transfers between phases are taken into account by the interfacial area concentration. In bubbly, slug and churn-turbulent flows the number density of small bubbles is one of the key parameters affecting this interfacial area concentration. However, there is no reliable correlation for the number density in a boiling two-phase flow system. In view of this, the bubble number density is studied in detail and a practical correlation has been developed.

First the bubble number density is formulated in terms of the differential transport equation for bubbles. From this equation it becomes clear that the active nucleation site density on a heated channel wall is the key parameter to predict the bubble number density.

Applying the pool boiling heat transfer correlation derived here, the active nucleation site density is obtained from experimentally measured values of water superheats and heat transfer coefficients for a wide range of system pressure, and the dimensionless active nucleation site density is correlated to the dimensionless cavity size and the density ratio. The pool boiling active nucleation site density correlation has been extended to the case of a forced convective nucleate boiling by using an effective liquid superheat rather than the actual wall superheat. The active nucleation site densities obtained in this way are in relatively good agreement with the experimental data available in literature.

I. INTRODUCTION

In a two-fluid model formulation of a two-phase flow system each phase is considered separately. Therefore, the formulation is expressed in terms of two sets (one for each phase) of conservation equations, i.e., in terms of six field equations: two continuity equations, two meomentum equations and two energy equations [1-8]. Since the macroscopic fields of one phase are not independent of those of the other phase, the interfacial interaction terms which couple the transport of mass, momentum and energy of each phase across the interfaces appear in the field equations. Therefore, the accuracy of analyses based on the two-fluid model is affected by the constitutive equations describing interfacial transport terms.

In addition to depending on the local transfer mechanism such as degree of turbulence in the vicinity of interfaces, the interfacial transport of mass, momentum and energy strongly depends on the interfacial area. Basically, interfacial interaction terms are proportional to the interfacial area concentration and to a driving force. The interfacial area concentration, defined as the interfacial area per unit volume of the mixture, characterizes the kinematic effects. Therefore, it must be related to the structure of the two-phase flow field. On the other hand, the driving forces for the interface transport characterize the local transport mechanism, and they must be modeled separately. Based on the mechanistic modeling, the driving forces were studied in detail [9].

Basic macroscopic parameters related to structure of two-phase flows, particularly of a dispersed flow, are the interfacial area concentration, the void fraction, particle number density and the shape factor. From geometrical considerations, the functional relationship between the interfacial area concentration and the other parameters can be derived. However, in order to use such a relation for the purpose of predicting the interfacial area concentration, one has to relate the number density to the characteristic fluid and flow variables. Information of this kind is desirable for predicting interfacial area concentration and has not been investigated in the literature.

It is the primary objective of this report to develop a reliable and simple predictive method for determining bubble number density in a forced convective nucleate boiling. To achieve this objective, a differential transport equation is introduced. This equation has source and sink terms, which take into account the wall nucleation, bulk heterogeneous nucleation and bubble collapse. The initial effort has been concentrated on the development of an empirical correlation for the surface nucleation rate.

II. BUBBLE NUMBER DENSITY BALANCE EQUATION

A. Interfacial Area Concentration Formulation

In general, the number density and the size spectrum of bubbles in a boiling channel change along the flow direction due to phase changes, coalescence, disintegrations and, finally, due to nucleations and collapses. The most general method to include these effects would be to introduce the general differential equation governing the number density of bubbles as a function of the bubble size distribution, position and time. This approach could be used in the solid particulate two-phase flow systems. However, it becomes highly complicated in the droplet and bubbly dispersed two-phase flow systems. Furthermore, the basic experimental data needed to go in this direction are grossly inadequate.

Instead of working with the complete size spectrum of bubbles, it is desirable to work with average radii [9]. Several of them are defined as follows:

$$\text{Sauter Mean Radius:} \quad r_{sm} = \frac{3B_b}{A_i} \tag{1.a}$$

$$\text{Drag Radius:} \quad r_d = \frac{3B_b}{4A_b} \tag{1.b}$$

$$\text{Equivalent Radius:} \quad r_v = \left(\frac{3B_b}{4\pi}\right)^{1/3} \tag{1.c}$$

$$\text{Surface Radius:} \quad r_s = \left(\frac{A_i}{4\pi}\right)^{1/2} \tag{1.d}$$

where A_i is the surface area of a typical bubble, A_b is the projected area of a bubble, and B_b is the volume of a typical bubble. For spherical bubbles the above defined radii are all equivalent. The number density N_b of bubbles, which is defined as the number of bubbles per unit volume of the two-phase mixture is given by

$$N_b = \frac{\alpha}{B_b} \tag{2}$$

and the interfacial area concentration, a_i is given by

$$a_i = A_i N_b \tag{3}$$

where α is the void fraction.

Using the above definitions, a_i can be expressed in a number of forms as follows:

$$a_i = \frac{3\alpha}{r_{sm}} = \frac{3\alpha}{r_v}\left(\frac{r_v}{r_{sm}}\right) = \frac{3\alpha}{r_v}\left(\frac{r_s}{r_v}\right)^2 \quad . \tag{4}$$

This equation shows that the interfacial area is a function of the void fraction, bubble size and shape factor. In view of Eqs. (1.c) and (1.d), the bubble size in Eq. (4) can be replaced by the number density N_b. Thus,

$$a_i = 4.84\left(\frac{r_s}{r_v}\right)^2 N_b^{1/3}\,\alpha^{2/3} \quad . \tag{5}$$

For an adiabatic flow Eq. (4) is useful, because the sizes of the bubbles may be determined from initial and boundary conditions. For a two-phase flow with a phase change, Eq. (5) may be more convenient, because the sizes of bubbles change due to phase changes.

Various shape factors appearing in Eq. (4) are important parameters for the interfacial area concentration. In fact, they relate various length scales at interfaces. It is evident from the definitions that for spherical particles,

$$\frac{r_s}{r_v} = \frac{r_v}{r_{sm}} = 1 \quad . \tag{6}$$

However, the deviations of these shape factors from unity become significant as deformations of fluid particles increase in the distorted particle and cap bubble regimes. They are extensively studied in Ref. [9]. Here we shall concentrate on the number density, N_b.

B. Bubble Number Density Balance Equation

Considering a boiling channel illustrated in Fig. 1, the local bubble number density balance equation can be expressed as follows:

$$\frac{\partial N_b}{\partial t} + \nabla \cdot (N_b \vec{v}_b) = \phi_{so} - \phi_{si} \tag{7}$$

where ϕ_{so} is the bubble source term due to the bulk nucleation, which is defined as the number of bubbles generated in the bulk liquid per unit time per unit volume of two-phase mixture, ϕ_{si} is the sink term due to bubble collapse, and $\vec{v}_b$ is the local bubble velocity.

For many engineering applications Eq. (7) can be simplified by means of proper averaging. The advantage of such an approach is two-fold. First, the variables appearing in the final equation will have explicit definitions in

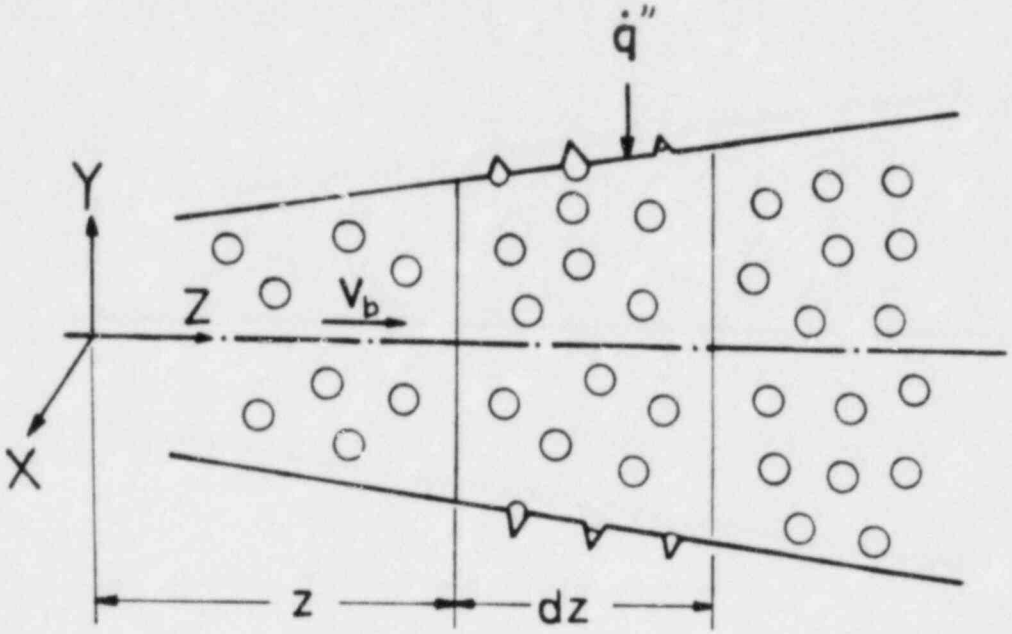

Fig. 1. A Schematic Representation of the Heated Channel Bubbly Flow

terms of averaged values. Consequently, it will be easy to compare predicted results with experimental data, which in two-phase flow are most often presented in terms of average values. Secondly, by means of space averages it will be possible to reduce the number of space variables and to treat the problem as one-dimensional one.

For the purpose of averaging, let us integrate the local bubble number density balance equation over the channel cross-sectional area, $A_c(z)$. Thus,

$$\iint_{A_c(z)} \frac{\partial N_b}{\partial t}\, dA + \iint_{A_c(z)} \nabla \cdot (N_b \vec{v}_b)\, dA = \iint_{A_c(z)} (\phi_{so} - \phi_{si})\, dA \quad . \qquad (8)$$

On the left hand side the first integral is transformed by means of the Leibnitz theorem over surfaces as

$$\iint_{A_c(z)} \frac{\partial N_b}{\partial t}\, dA = \frac{\partial}{\partial t} \iint_{A_c(z)} N_b\, dA - \int_{\xi(z)} \frac{\hat{n} \cdot (N_b \vec{v}_\xi)}{(\hat{n} \cdot \hat{n}_\xi)}\, d\xi \qquad (9)$$

whereas the second integral can be evaluated by means of the Gauss-Ostrogradskii divergence theorem over surfaces as

$$\iint_{A_c(z)} \nabla \cdot (N_b \vec{v}_b)\, dA = \frac{\partial}{\partial z} \iint_{A_c(z)} (N_b v_{bz})\, dA$$

$$+ \int_{\xi(z)} \frac{\hat{n} \cdot (N_b \vec{v}_b)}{(\hat{n} \cdot \hat{n}_\xi)}\, d\xi \quad . \tag{10}$$

In these equations, $\xi(z)$ is the intersection of channel wall with the cross-sectional plane, $\hat{n}$ is the unit vector normal to the channel wall, and $\hat{n}_\xi$ is the unit vector normal to ξ, located in the cross-sectional plane and directed away from the fluid.

Substituting Eqs. (9) and (10) in Eq. (8) and then rearranging, we obtain

$$\frac{\partial}{\partial t} \iint_{A_c(z)} N_b\, dA + \frac{\partial}{\partial z} \iint_{A_c(z)} (N_b v_{bz})\, dA = - \int_{\xi(z)} \frac{\hat{n} \cdot N_b(\vec{v}_b - \vec{v}_\xi)}{(\hat{n} \cdot \hat{n}_\xi)}\, d\xi$$

$$+ \iint_{A_c(z)} (\phi_{so} - \phi_{si})\, dA \quad . \tag{11}$$

In terms of area-averaged quantities, Eq. (11) can be expressed as

$$\frac{\partial}{\partial t} (A_c \langle\langle N_b \rangle\rangle) + \frac{\partial}{\partial z} (A_c \langle\langle N_b v_{bz} \rangle\rangle) = - \int_{\xi(z)} \frac{\hat{n} \cdot N_b(\vec{v}_b - \vec{v}_\xi)}{(\hat{n} \cdot \hat{n}_\xi)}\, d\xi$$

$$+ A_c(\langle\langle \phi_{so} \rangle\rangle - \langle\langle \phi_{si} \rangle\rangle) \tag{12}$$

where the area averaged value of any quantity F is defined by

$$\langle\langle F \rangle\rangle (z,t) \equiv \frac{1}{A_c} \iint_{A_c(z)} F(x,y,z,t)\, dA \quad . \tag{13}$$

The introduction of averaged system variables into the number density balance equation cannot eliminate all the effects of the multi-dimensionality because the average of a product is not the same as the product of the average of the variables N_b and v_{bz}. That is

$$\langle\langle N_b v_{bz} \rangle\rangle \neq \langle\langle N_b \rangle\rangle \cdot \langle\langle v_{bz} \rangle\rangle \tag{14}$$

unless one of the variables is constant over the cross-sectional plane. However, such a relation between the average of a product and the product of the averages of the variables N_b and v_{bz} can be accomplished by introducing the covariance and correlating it to other macroscopic variables, see for example, Ref. [10]. The covariance is defined by

$$\text{Cov}\,(N_b\, v_{bz}) = \langle\langle N_b\, v_{bz}\rangle\rangle - \langle\langle N_b\rangle\rangle\, \langle\langle v_{bz}\rangle\rangle \quad . \tag{15}$$

In view of Eq. (15), Eq. (12) can be expressed in the following form

$$\frac{\partial}{\partial t}\,(A_c\, \langle\langle N_b\rangle\rangle) + \frac{\partial}{\partial z}\,(A_c\, \langle\langle N_b\rangle\rangle\, \langle\langle v_{bz}\rangle\rangle) = -\int_{\xi(z)} \frac{\hat{n}\cdot N_b(\vec{v}_b - \vec{v}_\xi)}{(\hat{n}\cdot\hat{n}_\xi)}\, d\xi$$

$$+ A_c\,(\langle\langle \phi_{so}\rangle\rangle - \langle\langle \phi_{si}\rangle\rangle) - \frac{\partial}{\partial z}\,[A_c\, \text{Cov}\,(N_b\, v_{bz})] \quad . \tag{16}$$

It should be noted that $-\hat{n}\cdot N_b(\bar{v}_b - \bar{v}_\xi)$ is the bubble flux at the boundaries of the flow channel. There can be two reasons for this. One is due to the introduction of bubbles into the flow channel through permeable channel wall, and the other is due to bubble generation from the active nucleation sites on heated boundaries. Both of them can be considered as bubble generation at the external boundaries. Introducing N_a, the bubble generation centers per unit area of the channel wall, and f, the bubble generation frequency one can express the bubble flux term as follows:

$$-\hat{n}\cdot N_b(\vec{v}_b - \vec{v}_\xi) = N_a\, f \quad . \tag{17}$$

Introducing the bubble flux expression given by Eq. (17) in Eq. (16), the bubble number density balance equation can be expressed as

$$\frac{\partial}{\partial t}\,(A_c\, \langle\langle N_b\rangle\rangle) + \frac{\partial}{\partial z}\,(A_c\, \langle\langle N_b\rangle\rangle\, \langle\langle v_{bz}\rangle\rangle) = -\int_{\xi(z)} \frac{N_a\, f}{(\hat{n}\cdot\hat{n}_\xi)}\, d\xi$$

$$+ A_c(\langle\langle \phi_{so}\rangle\rangle - \langle\langle \phi_{si}\rangle\rangle) - \frac{\partial}{\partial z}\,[A_c\, \text{Cov}\,(N_b\, v_{bz})] \quad . \tag{18}$$

Equation (18) is the one-dimensionalized, area-averaged bubble number density transport equation, which is applicable for a channel with variable cross-sectional plane. For a constant cross-sectional area channel, it can be further simplified to

$$\frac{\partial \langle\langle N_b \rangle\rangle}{\partial t} + \frac{\partial}{\partial z}\left(\langle\langle N_b \rangle\rangle \langle\langle v_{bz} \rangle\rangle\right) = \langle \phi_w \rangle + \langle\langle \phi_{so} \rangle\rangle - \langle\langle \phi_{si} \rangle\rangle$$

$$- \frac{\partial}{\partial z} \mathrm{Cov}\left(N_b\, v_{bz}\right) \qquad (19)$$

where $\langle \phi_w \rangle$ is the perimeter-averaged bubble generation rate from active nucleation sites at the channel wall, which is defined by

$$\langle \phi_w \rangle = \frac{1}{A_c} \int_{\xi} (N_a\, f)\, d\xi = \frac{\langle N_a \rangle\, f\, \xi}{A_c} \qquad (20)$$

where the frequency f has been assumed to be uniform.

In order to be able to use the one-dimensional form of the bubble number density balance equation expressed by Eq. (19), one should have information about the source and sink terms due to the wall and bulk liquid nucleation, and the bubble collapse rate together with the bubble distribution, which will be taken into account by the covariance term appearing in Eq. (19).

C. Bulk Liquid Nucleation

In general, bubble nucleation in the bulk liquid may be either of the homogeneous or heterogeneous types. Designating the homogeneous nucleation rate by ϕ_{ho} and the heterogeneous nucleation rate by ϕ_{he}, one can write

$$\phi_{so} = \phi_{ho} + \phi_{he} \quad . \qquad (21)$$

Several theories based on statistical mechanics have been proposed to account for homogeneous nucleation in the pure liquid. One approach using classical rate theory [11], presumes that numerous molecules have the activation energy required for existence in the vapor phase. These energetic molecules could combine through collisions to form a cluster, which is then a vapor bubble. Theories of this type indicate that the rate of homogeneous nucleation is an extremely sensitive function of the bulk liquid superheat. At lower superheats the homogeneous nucleation rate is not significant, but it increases rapidly as the superheat is increased. However, the homogeneous nucleation theories yield extremely high liquid superheats for nucleation in a pure liquid. In fact, the superheat requirement for homogeneous nucleation is much greater than any experimental value which has been measured for water, even under very carefully controlled conditions [12], for example, 105°C for water at 1 atm. pressure. Such high superheats are contrary to experimental observations with real systems.

In a real system, the liquid contains foreign particles and dissolved gas which could act as nuclei. The predicted nucleation superheats would be considerably less in the presence of a pre-existing gas phase. This form of heterogeneous nucleation, ϕ_{he}, implies that vapor formation would be noted at

random points where the nuclei happen to be located. This type of bubble formation becomes important, even with an adiabatic channel flow where drastic depressurization occurs. For example, it might be very significant for the discharge of flashing steam-water mixtures through short nozzles or orifices [13].

In a system with heat addition, however, bubbles form at specific locations associated with the heated surface, not in the fluid. Furthermore, it has been found by macroscopic observations that these locations are small imperfections or cavities on the heated surface [14]. For a boiling system, then homogeneous and heterogeneous bulk liquid nucleation are dominated by cavity nucleation, $\langle\phi_w\rangle$. It should be noted, however, that for those cases where flashing is important, such as during rapid acceleration and pressure changes, the proper constitutive relation for the phase change, i.e., for $\langle\langle\phi_{he}\rangle\rangle$, should be used. In this report, however, the initial effort will be concentrated on developing a constitutive relation for the wall nucleation rate $\langle\phi_w\rangle$.

D. Bubble Re-Condensation Rate

In general, reduction in bubble number density, which was taken care of by the sink term, $\langle\langle\phi_{si}\rangle\rangle$, may be due to either coalescence of bubbles into a larger bubble or re-condensation of bubbles in the subcooled bulk fluid. Here the effort has been concentrated on determining the re-condensation rate of generated bubbles. The coalescence is assumed to be insignificant up to the void fraction of 0.3 beyond which the flow regime transition to the slug or churn-turbulent flow occurs.

The bubble generation along the length of a heated channel is shown qualitatively in Fig. 2. The existence of two regions, as shown in Fig. 2, has been confirmed through several experimental investigations [15-17]. In region I, the surface temperature and, therefore, the liquid temperature in the vicinity of the heated surface are high enough to permit nucleation of small bubbles. But, due to the high subcooling prevailing at the liquid core, small bubbles grow and collapse while still attached to the surface and cannot penetrate far into high subcooled bulk flow until the point B is reached. At this point the thermal, as well as hydrodynamic, conditions are such that bubbles grow and detach, condensing only to some degree as they pass through the slightly subcooled liquid. The bubble number density and the void fraction increase with the length from the transition point, B, although the liquid bulk temperature is still below the corresponding saturation temperature. Region I is of little significance as far as the net bubble generation is concerned, and in this region

$$\langle\langle\phi_{si}\rangle\rangle \simeq \langle\phi_w\rangle \quad . \tag{22}$$

For all purposes, therefore, the point B can be regarded as the point of net bubble generation. Due to its importance, a great deal of attention has been paid to determine the location of this point as a function of the system parameters [16-24]. Our major problem, however, is to determine the bubble recondensation rate in this region, which is essential in Eq. (19).

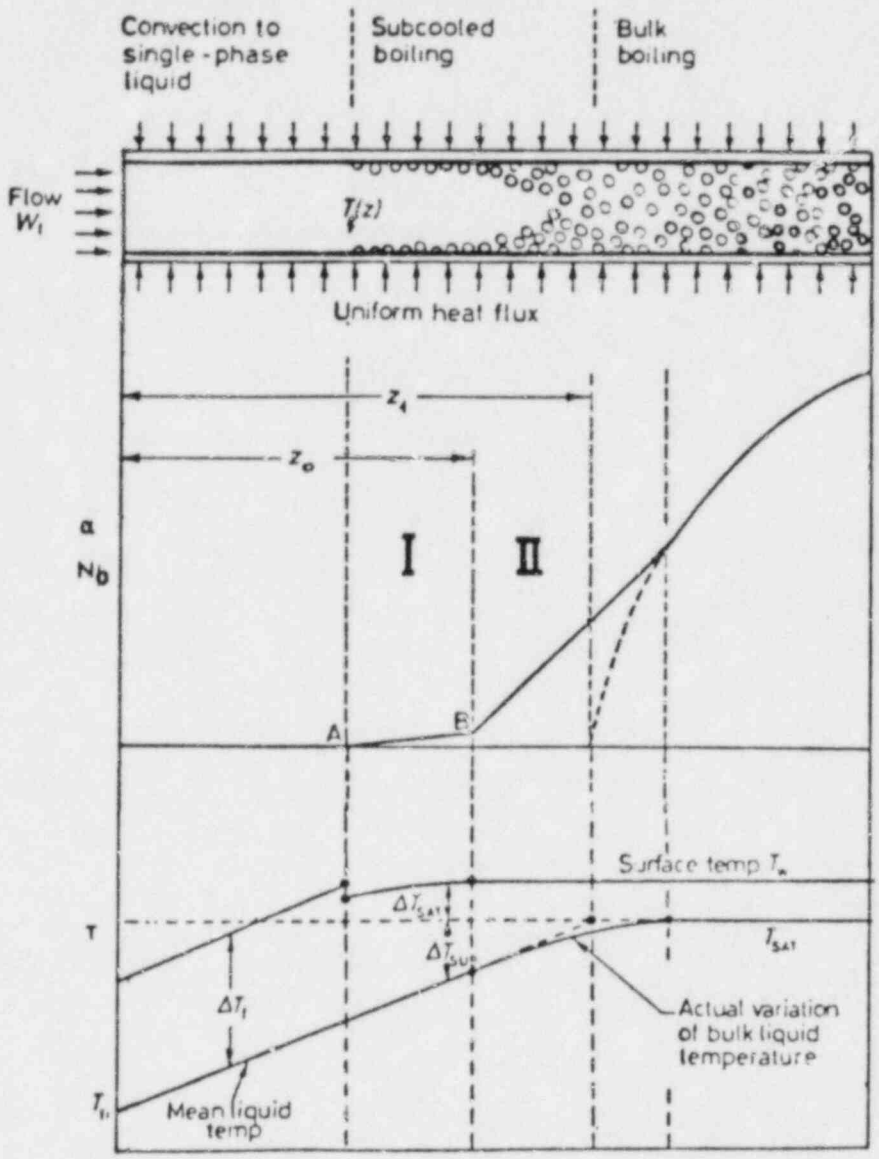

Fig. 2. Schematic Representation of Void Fraction (α), Number Density (N_b), Liquid Temperature (T_f), and Surface Temperature (T_w) in Axial Direction (z)

In Region II, the bulk liquid is still subcooled when the bubbles are generated and detached into the main stream. Some of the bubbles generated and detached at the surface will recondense in the subcooled bulk liquid. The fraction of re-condensation can be obtained by comparing the rates of net vapor generation and evaporation at the surface. In order to make an estimate of these two rates, we can assume that the rate of evaporation at the surface will be proportional to the total heat flux, $\dot{q}''$, minus the single phase convective heat flux, $\dot{q}''_{sp}$, whereas the rate of net vapor formation will be proportional to the amount of energy that is used to increase vapor flow. Consequently, the fraction of bubbles that recondense, η, can be estimated as follows:

$$\eta = 1 - \frac{\frac{d}{dz}\{G_g[i_{fg} + C_{pf}(T_{sat} - T_f)]\}}{(\dot{q}'' - \dot{q}''_{SP})\left(\frac{\xi}{A_c}\right)} \tag{23}$$

here $\dot{q}''$ is the total wall heat flux, whereas $\dot{q}''_{SP}$ is the convective heat flux due to the single phase liquid convection and the sink term becomes

$$\langle\langle\phi_{si}\rangle\rangle = \eta \langle\phi_w\rangle \tag{24}$$

where G_g is the vapor mass velocity, and T_f is the liquid bulk temperature.

The right hand side of Eq. (23) can be evaluated through the use of balance equations. Consider a steady, one-dimensional flow of a two-phase mixture with constant properties and assume that the effects of the kinetic and potential energies can be neglected. Then we have the energy equation for the mixture

$$\frac{d}{dz}(G_g\, i_g + G_f\, i_f) = \frac{\dot{q}''\,\xi}{A_c} \tag{25}$$

and the conservation of mass for the mixture

$$\frac{d}{dz}(G_g + G_f) = 0 \tag{26}$$

where i_g and i_f are the vapor and bulk liquid enthalpies, respectively.

Using Eqs. (25) and (26) in Eq. (23), it can be shown that

$$\eta = \frac{G\, C_{pf}\left(\frac{dT_f}{dz}\right) - \dot{q}''_{SP}\left(\frac{\xi}{A_c}\right)}{(\dot{q}'' - \dot{q}''_{SP}) \cdot \left(\frac{\xi}{A_c}\right)} \quad . \tag{27}$$

It is important to note that the expression derived for the prediction of η satisfies two limiting cases. Until point B in Fig. 2 is reached, the total energy supplied to the subcooled liquid is used for increasing the temperature of the liquid without net vapor generation. Therefore, in this region η approaches unity in Eq. (27). On the other hand, in the saturated nucleate boiling region $dT_f/dz = 0$. Therefore, η becomes zero in Eq. (27).

It can be seen from Eq. (27) that in order to evaluate $\langle\langle\phi_{si}\rangle\rangle$, it is necessary to determine first the axial liquid bulk temperature distribution $T_f(z)$. In Refs. [25-27], the axial temperature distribution for subcooled

boiling has been approximated by some functions that satisfy the physical boundary conditions. It was shown in Ref. [27] that the exponential or the hyperbolic tangent approximation for the temperature profiles gave satisfactory results when compared to available experimental data. In view of its simplicity, we shall introduce here the exponential approximation expressed as

$$\frac{T_f(z) - T_o}{T_{sat} - T_o} = 1 - \exp\left(-\frac{z - z_o}{\Delta\ell}\right) \tag{28}$$

where the characteristic length $\Delta\ell$ is given by

$$\Delta\ell = z_1 - z_o = \left(\frac{A_c}{\dot{q}''\ \xi}\right) C_{pf}\ G(T_{sat} - T_o) \quad . \tag{29}$$

In these relations, z_o is the axial coordinate at the point of practical incipient vapor formation, z_1 is the axial coordinate at point $T_f = T_{sat}$, assuming thermodynamic equilibrium, and T_o is the liquid bulk temperature at z_o [24].

With this temperature profile, η can be calculated from Eq. (27) as

$$\eta = 1 - \frac{\left(\frac{T_f - T_o}{T_{sat} - T_o}\right)}{1 - \left(\frac{\dot{q}''_{SP}}{\dot{q}''}\right)} \quad . \tag{30}$$

This expression is general if we use the standard single phase heat transfer correlation for $\dot{q}''_{SP}$ and two-phase flow heat transfer correlation. However, this will lead to a highly complicated correlation for $\langle\langle\phi_{si}\rangle\rangle$. Therefore, it is desirable to obtain a simple expression which satisfies overall physical phenomenon.

First consider the fully developed subcooled boiling region where $\dot{q}''_{SP}$ is insignificant in comparison with the nucleate boiling heat flux. Under this approximation Eq. (30) reduces to

$$\eta = \frac{T_{sat} - T_f}{T_{sat} - T_o} \quad . \tag{31}$$

This relation satisfies the limiting condition of saturated boiling. Since when T_f approaches to T_{sat} η approaches to zero, indicating that the amount of re-condensation becomes zero.

Second consider the neighborhood of net vapor generation point in the relatively high subcooling boiling region. In this region, the single phase convective heat transfer is significant in relation to the nucleate boiling heat transfer. Thus, in Eq. (30) $\dot{q}''_{sp}$ should play a major role in determining η or the re-condensation rate. However, as T_f approaches to T_o

$$\langle\langle \phi_{si} \rangle\rangle \to \langle \phi_w \rangle \tag{32}$$

because all bubbles nucleated at the wall should immediately re-condense. The above equation implies that

$$\eta \to 1 \text{ as } T_f \to T_o \quad . \tag{33}$$

Now, in terms of the local heat flux, η can also be expressed as

$$\eta = \frac{\dot{q}''_{cond.}}{\dot{q}''_{boil}} \tag{34}$$

where $\dot{q}''_{boil}$ is the nucleate boiling portion of the total wall heat flux, and $\dot{q}''_{cond.}$ is the condensation heat flux at the outer edge of the bubble boundary layer. Since $\dot{q}''_{cond.}$ is mainly governed by the single phase heat transfer in the highly subcooled liquid core where steep liquid temperature gradient exists outside the bubble boundary layer. In this case, it is expected that $\dot{q}''_{cond.} \sim (T_{sat} - T_f)$. The limiting condition of η at $T_f = T_o$ and this relation imply that η in this region should be as follows:

$$\eta = \frac{T_{sat} - T_f}{T_{sat} - T_o} \quad . \tag{35}$$

It is interesting to note that this equation has the same form as Eq. (31). Therefore, from these two limiting conditions it may be concluded that the general expression for η can be given approximately by Eq. (31).

In view of Eqs. (24) and (31), the sink term can be expressed as

$$\langle\langle \phi_{si} \rangle\rangle = \left(\frac{T_{sat} - T_f}{T_{sat} - T_o} \right) \langle \phi_w \rangle \text{ for } T_o \leq T_f \leq T_{sat} \quad . \tag{36}$$

It is noted that the above expression for the condensation rate has been obtained by considering a normal case of boiling flow using a one-dimensional formulation. Because of this, the applicability of Eq. (36) is limited to one or quasi-one-dimensional formulation and to boiling flow, i.e., $\langle \phi_w \rangle > 0$.

This constitituve relation can be extended to outside of the above limitations under special cases only. For example, such as the bulk condensation due to pressurization where the bubble size changes are more important than the changes in tne number density. However, it may not be applied to the condensing flow where heat is removed from the wall and the subcooled liquid boundary layer exists near the wall.

E. Summary and Methodology

Combining the bubble number density sink term defined by Eq. (36) and the wall nucleation source term defined by Eq. (20), and substituting the resulting equation together with Eq. (21) in Eq. (19), the final form of the bubble number density balance equation can be given by

$$\frac{\partial \langle\langle N_b \rangle\rangle}{\partial t} + \frac{\partial}{\partial z}\left(\langle\langle N_b \rangle\rangle \langle\langle V_{bz} \rangle\rangle\right) = \left(\frac{T_f - T_o}{T_{sat} - T_o}\right)\left(\frac{\langle N_a \rangle \langle f \rangle \xi}{A_c}\right)$$

$$+ \langle\langle \phi_{he} \rangle\rangle + \langle\langle \phi_{ho} \rangle\rangle - \frac{\partial}{\partial z} \mathrm{Cov}\left(N_b V_{bz}\right) \quad . \tag{37}$$

From this equation, it is obvious that in order to be able to use the one-dimensional bubble number density equation, one should have information about heterogeneous and homogeneous bulk liquid nucleation rates identified by $\langle\langle \phi_{he} \rangle\rangle$ and $\langle\langle \phi_{hc} \rangle\rangle$, respectively, together with the bubble generation frequency, $\langle f \rangle$, and the active nucleation site density, $\langle N_a \rangle$, because ξ and A_c appearing in Eq. (37) are geometric parameters characterizing the heated flow channel.

As discussed above, the superheat requirement for homogeneous nucleation is much greater than any experimental value which has been measured for water even under very carefully controlled conditions, and it was concluded that, for water at least, homogeneous nucleation could be discounted as a mechanism for vapor formation under normal conditions. It was also pointed out that the heterogeneous bulk nucleation might be significant for the flow channels where drastic depressurization occurs. For a heated channel, however, the major bubble nucleation source will be due to the wall nucleation, that is due to the first term on the right hand side of Eq. (37). Even in flashing flow, at least the initial vaporization is expected to be dominated by the wall nucleations. In view of these, first the active nucleation site density, $\langle N_a \rangle$, will be correlated in this study.

In a microscopic sense, the bubble nucleation process from cavities is similar in both the pool boiling and the convective nucleate boiling. In both cases, to maintain nucleate boiling on a surface, it is necessary that the wall superheat exceeds a critical value for a specified system pressure. In view of this mechanistic similarity, it is reasonable to start with the pool boiling studies. A number of pool boiling data providing quantitative information on active nucleation site density have been accumulated over the years. It should be noted, however, that none of the experiments, when investigating the effect of pressure on pool boiling performance, simultaneously

counted active nucleation site density. Furthermore, the pressure ranges covered by these data are far short of being sufficient to directly arrive at a reliable correlation. Most of the existing data have been obtained at subatmospheric pressures. Very few data exist for higher pressures beyond 1 atm.

Due to a lack of experimental nucleation site density data over a wide range of pressures, first, heat transfer data will be studied in Section III. Then, the results of heat transfer studies in the pool boiling will be used in Section IV to arrive at an active nucleation site density correlation.

III. HEAT TRANSFER IN POOL BOILING

A. Introduction

Heat transfer in pool boiling has been investigated extensively for many years and numerous equations have been proposed for correlating experimental data. Because the high heat flux densities in nucleate boiling were attributed to bubbles which induce locally a strong stirring action of the liquid near the heating surface in most of the early correlations [28-36], the heat transfer is determined by the agitating action of the bubbles. They may all be written in the general dimensionless form of

$$Nu = \text{Const.}\ R_e^m\ P_r^n \quad . \tag{38}$$

The differences among them stems from the way in which the hydrodynamic process of stirring of the liquid in the vicinity of the heating surface is taken into account. In the dimensional form, Eq. (38) can be expressed in the form

$$\dot{q}'' = \text{Const.}\ (T_w - T_{sat})^p \tag{39}$$

where the value of the exponent varies between 2 and 4 and the constant depends on the thermophysical properties of the vapor and the liquid, as well as on the solid-liquid combination.

The major drawback of this type of correlation consists in the fact that the structure of the heating surface is not taken into account. In fact, it was noted and discussed in Refs. [37-38] that a generalized correlation cannot be expected to hold unless the correlation takes into account the nucleating characteristic of the heating surface and the effect of the bubble nucleation site density. With the experiments, which provided quantitative information on the active nucleation site density, it was shown in Refs. [39-43] that instead of expressing the heat flux density in terms of the liquid superheat temperature difference $(T_w - T_{sat})$ as in Eq. (39), it was also possible to express it in terms of the number of active nucleation site density N_p alone, thus

$$\dot{q}'' = \text{Const.}\ N_p^a \quad . \tag{40}$$

The first part of Table I lists some empirical correlations of active nucleation site density with heat flux. It can be seen that, although a wide variety of liquids and surfaces were used, the range of the exponent index for N_p is surprisingly narrow with a range of 1/3 and 1/2 for different metals and 0.73 for glass. That means the power index in the correlation of site population and heat flux is independent of surface finish for metals. However, it does not imply that heat transfer is independent of surface finish. First of all, the constant appearing in Eq. (40) is still a function of surface finish. Furthermore, as demonstrated in Refs. [37-44], the surface finish also affects the temperature difference as well as the active nucleation site density.

More detailed experimental information has conclusively shown that the heat flux density in nucleate boiling is not a single-valued function of the superheat temperature difference, but depends upon both the superheat and the number of active nucleation site density [44-50]. This series of correlations can be represented by

$$\dot{q}'' = \text{Const.}\ (T_w - T_{sat})^b\ N_p^c \tag{41}$$

where Const. depends on the thermophysical properties of the vapor and the liquid. Such a relationship is reasonable from a physical standpoint, since it related $\dot{q}''$ to surface condition -- a variable neglected in boiling heat transfer correlation of the type represented by Eq. (39). The most representative empirical correlations of active nucleation site density with heat-flux and the superheat are listed in the second part of Table I. The range of the exponent index for $(T_w - T_{sat})^b$ varies between 1.0 and 3.07 while c varies between 0.25 and 0.68. For the purpose of comparison of existing correlations, Fig. 3 is reproduced from Ref. [51] and shows the effect of exponent in different correlations.

Two-parameter expressions similar to Eq. (41) were also derived from theoretical considerations [51-52]. In Ref. [51], a hydrodynamic model of stagnation laminar flow was proposed, and via dimensional considerations, an equation for the heat transfer coefficient was obtained. In Ref. [52], however, the heat-transfer coefficient was obtained on the basis of an analogy with turbulent forced convection, replacing the buoyancy force in the equation for the free convection by the difference between the liquid mass density and the mass density of the two-phase mixture. The value of the exponents were, however, different with b = 1 and c = 1/2 obtained in Ref. [51] and b = 5/3 and c = 1/3 obtained in Ref. [52].

From this brief summary on the existing work on the relationship between the heat transfer and the active nucleation site density, it can be concluded that for boiling of different liquids and for different surface conditions there exists a similar variation of site density with heat flux and the wall superheat. From Eq. (41) it follows that

Table I. Active Nucleation Site Density Correlations

a) $\dot{q}'' = \text{Const.}\ N_p^a$, Eq. (40)

Author(s) [Reference]	Heater	Surface-Fluid Combination	Heat Flux Range (Btu/hft^2)	Exponent a
Jacob [28]	Flat Plate	Chromium Plated-water	$\dot{q}'' < 18{,}000$	1.0
Gaertner & Westwater [39]	Flat Plate (2" diameter)	Copper-Ni-H_2O Solution	$7{,}680 < q < 317{,}000$	0.47
Kirby & Westwater [40]	Flat Plate (2" square)	Carbon Tetrachloride - Copper	$\dot{q}'' < 90{,}300$	
		Methanol - Copper	$\dot{q}'' < 142{,}000$	0.50
		Carbon Tetrachloride - Glass		0.73
Gaertner [41]	Flat Plate (2" diameter)	Platinum - Water Copper - Water	$10{,}500 < \dot{q}'' < 58{,}600$	0.67
Semeria [40]	Wires	Water	$3 < P < 100$ atm.	0.50

Table I. Active Nucleation Site Density Correlations (Cont'd)

b) $\dot{q}'' = \text{Const.}\ (T_w - T_s)^b\ N_p^c$, Eq. (41)

Author(s) [Reference]	Heater	Surface-Fluid Combination	Heat Flux Range (Btu/hft^2)	Exponent b	Exponent c
& Myers	Flat Plate (3" diameter)	Copper - Water Copper-Organic Liquids	$\dot{q}'' < 19{,}000$	1.0	0.33
Nishikawa [44]	Flat Plate	Brass-Water Solutions	$\dot{q}'' < 13{,}600$	1.0	0.33
Yamagata & Nishikawa [45]	Flat Plate (10 cm diameter)	Brass-Water Solutions	$\dot{q}'' < 11{,}600$	1.5	0.25
Orell [50]	Wires (0.008" diameter)	Water & Organic Liquids	For Normal Case For S-Shape Curve	1.0 1.0	0.5 0.5-0.68
Helad, Ricklis & Orell [49]	Flat Plate (2" diameter)	Brass-Organic Liquids (Artificial Cavities)	$3{,}2300 < \dot{q}'' < 19{,}840$ $10{,}500 < \dot{q}'' < 81{,}500$	1.67 3.07	0.42 0.606
Tien [51]	Horizontal Surface	Theoretical, Inverted Plane Stagnation Flow Model		1.0	0.5
Zuber [52]	Horizontal Surface	Theoretical, Turbulent Natural Convection Model		1.57	0.33

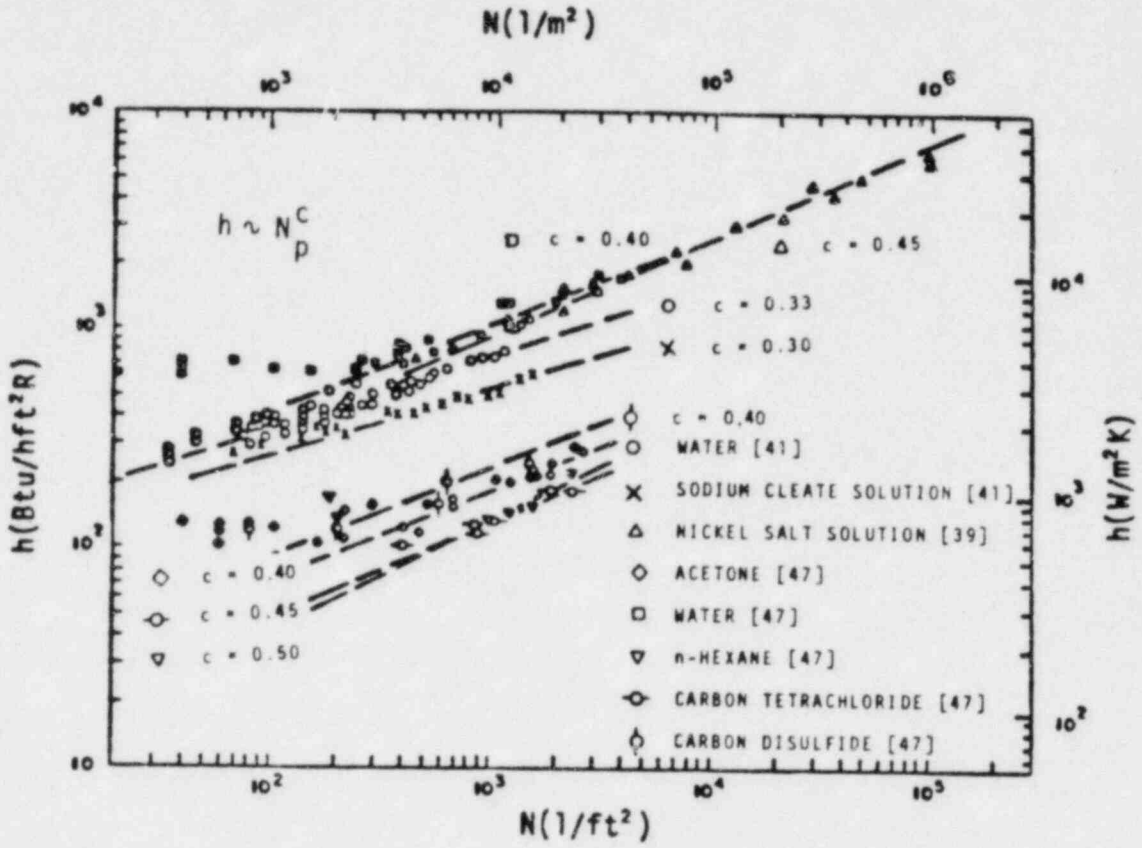

Fig. 3. Variation of Heat Transfer Coefficient with Active Nucleation Site Density [51]

$$N_p = \text{Const.}\ \dot{q}''^{1/c}\ (T_w - T_{sat})^{-b/c} \quad . \tag{42}$$

However, it cannot be directly used for the purpose of calculating N_p as long as $\dot{q}''$ and $(T_w - T_{sat})$ are not measured simultaneously.

In what follows, we shall follow a different path in predicting the active nucleation site density in nucleate boiling. For this purpose, in this section, we shall correlate existing pool boiling data in the form of Eq. (42) by starting with a forced-convection heat transfer model. In the following section, this correlation will be used to correlate the active nucleation site density to the active site size and the fluid properties as follows:

$$N_p = f(R_c, \text{fluid properties}) \tag{43}$$

where R_c is the critical cavity radius.

A correlation in the form of Eq. (43) is not expected to hold exactly for each fluid-surface combination but it will certainly serve to approximately predict a number of nucleation sites in terms of practically measureable or calculable quantities.

B. Model

In order to discuss the heat transfer to a boiling liquid, it is important to describe the hydrodynamic field of the fluid adjacent to the heated surface. It should be noted, however, that a simple description can be limited only to the relatively low heat-flux range, because in the high-heat flux region bubbles begin to merge and the activity is not as orderly as the discrete bubbling region and, therefore, is difficult to model.

If we consider a single nucleation site, following the nucleation from a cavity, the bubble starts growing in a superheated liquid film while it is still attached to the heated surface. During this growth, the bubble pushes the surrounding liquid outward. Although the bubble slightly deforms in this period, the motion in the liquid will be radial, Fig. 4. The liquid convection associated with the bubble growth can be analyzed as a source flow. Conceptual models, based on the source flow, were formulated in Refs. [52] and [54] for nucleate boiling of subcooled liquids and in Ref. [55] for liquids at saturation.

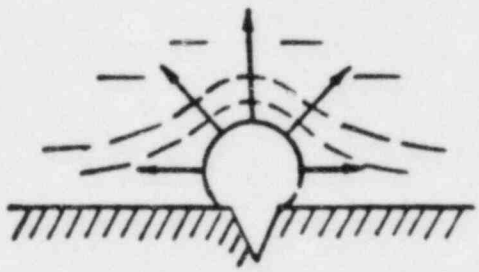

Fig. 4. The Source Flow Associated with the Growing Bubble [52]

Eventually, the bubble grows to the point where it departs from the heating surface due to the buoyant and drag forces. Immediately after the detachment, the lower surface of the bubble reenters, Fig. 5, and deforms the bubble in a lenticular shape. Liquid is entrained in the wake of the detaching and rising spheroidal bubble, i.e., the wake flow. This causes upflow of the hot liquid following the bubble. Colder liquid comes in contact with the heated surface and gets heated again until it is hot enough to sponsor the growth of a new consecutive bubble. This new bubble grows until the departure and the process described above is repeated. A bubble column is thus formed by bubbles successively rising from a nucleating center. The period prior to the appearance of the second bubble is called the waiting period, and the period between appearance and the departure of a bubble is called the growth time. Waiting time depends upon the local heat-flux, thermal fluctuations in the liquid and the nucleation center size. The growth time depends on the local superheat and on the local hydrodynamic condition.

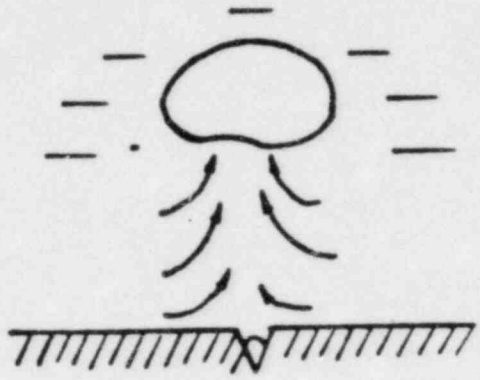

Fig. 5. The Wake Flow Associated with Departing Bubble [52]

From the foregoing it can be concluded that for boiling on a horizontal surface the liquid flow pattern in the vicinity of a nucleation center continuously oscillates between the source flow and the wake flow. For boiling on a vertical surface, however, the liquid flow pattern should be different from the flow patterns discussed above. In particular, the density differential which sets up the motion in the case of boiling on a horizontal surface [52, 56] cannot be effective in the case of boiling on a vertical surface. However, the agitating effect of the source flow will be similar in both cases. Furthermore, it should be noted that the degree of agitation of the source flow in subcooled boiling is independent of the degree of subcooling [52, 55, 57]. It is identical to the liquids at saturation temperature.

Since we are trying to obtain a practical correlation which can be used for the nucleate boiling on both the horizontal and vertical surfaces and, since we want to use the correlation for the subcooled as well as the saturated nucleate boilings, we shall adopt the source flow model in the forthcoming correlation.

C. Heat Transfer Correlation

In view of the foregoing discussion, the heat transfer data gathered from a wide variety of sources were correlated on the basis of the source flow model. The liquid motion near the heat transfer surface in the vicinity of a nucleation center is approximated by a radial motion having a characteristic dimension of s/2 where s is the average distance between neighboring active nucleation centers. Therefore, the radius of an influence domain of a growing bubble would be s/2. While it is known that the active nucleation sites are distributed rather randomly over the heated surface, the average bubble spacing is directly related to active nucleation site density [55] as

$$s = N_p^{-1/2} \quad . \tag{44}$$

Since nucleate boiling studies deal with the formation and detachment of vapor bubbles, the heat transfer data were fitted with the convective heat transfer correlation having a form of

$$Nu = \text{Const.}\ Re^{m}\ Pr^{n}\ (D_d/s)^{p} \quad . \tag{45}$$

The Nusselt number is defined as

$$Nu = \frac{hs}{k_f} \tag{46}$$

where k_f is the thermal conductivity of the liquid phase.

The dimensionless group (D_d/s) is the ratio of the bubble diameter at departure and the size of the average bubble spacing, which is expressed in terms of the active nucleation site density, N_p, given by Eq. (44). In almost all of the boiling heat transfer studies, the Fritz equation [58] has been used for the bubble departure diameter. However, a comparison of the Fritz equation with the available experimental water data in Appendix A shows that the Fritz equation yields a good agreement only around atmospheric pressure. For high pressure use, the Fritz equation has been modified based on experimental water data, see Fig. 6. Thus the following bubble departure expression is proposed:

$$D_d = 0.0012 \left(\frac{\Delta\rho}{\rho_g}\right)^{0.9} D_{dF} \tag{47}$$

Here D_{df} is the bubble departure diameter calculated through the use of the Fritz equation given by

$$D_{dF} = 0.208\ \theta \left(\frac{\sigma}{g\Delta\rho}\right)^{1/2} \tag{48}$$

where θ is the contact angle, and σ is the surface tension. It should be noted that D_d approaches zero as pressure approaches the critical pressure. On the other hand, at near atmospheric pressures, D_d essentially reduces to the value obtained from the Fritz equation, D_{dF}.

The Reynolds number appearing in the proposed heat transfer correlation, Eq. (45), is defined as

$$Re = \frac{\rho_f\ \bar{v}_f\ s}{\mu_f} \tag{49}$$

where $\bar{v}_f$ is the characteristic mean liquid velocity associated with a growing bubble.

The radial liquid velocity due to the source flow around one growing bubble was derived in Refs. [53] and [54], and it was given by

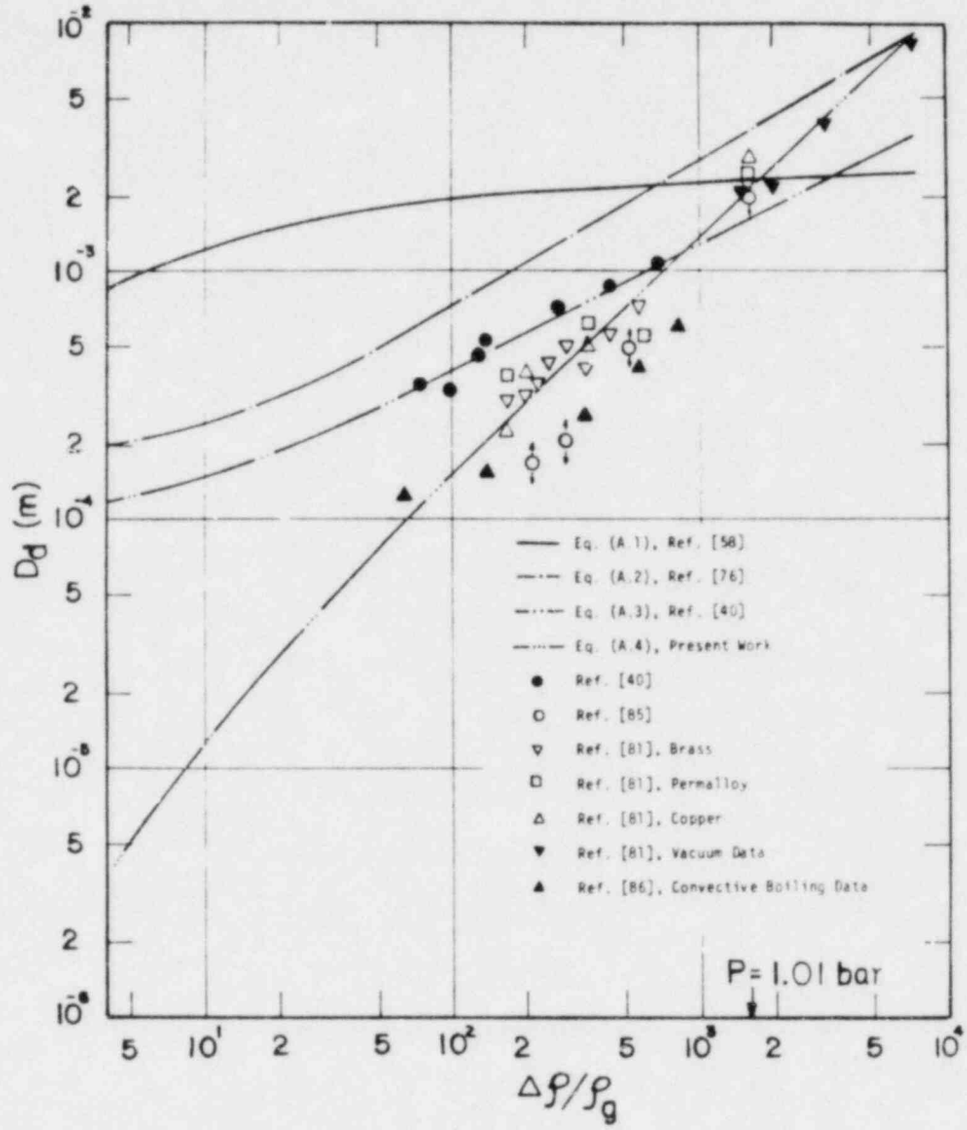

Fig. 6. Bubble Departure Diameter vs. Density Ratio (Water)

$$v_f(r) = \frac{R^2 \dot{R}}{r^2} \tag{50}$$

where R and $\dot{R}$ are the instantaneous bubble radius and the radial growth velocity, respectively. It was shown [52, 55] that Eq. (50) can be used to estimate a mean velocity due to the source flow of the liquid within a bubble influence domain, $R \leq r \leq s/2$. Therefore, the mean velocity is defined by

$$\bar{v}_f = \frac{1}{\left(\frac{s}{2} - R\right)} \int_R^{s/2} \frac{R^2 \dot{R}}{r^2} \, dr \tag{51}$$

then

$$\bar{v}_f = \frac{2\,R\,\dot{R}}{s} \quad . \tag{52}$$

Finally, using the product ($2R\dot{R}$) expression derived in Refs. [52] and [57], one obtains

$$\bar{v}_f = 1.27 \left[\frac{\rho_f\, C_{pf} \sqrt{a_f}\, (T_w - T_{sat})}{\rho_g\, i_{fg}} \right]^2 \Bigg/ s \quad . \tag{53}$$

In view of Eqs. (44), (46), (49) and (53), the heat transfer relation becomes

$$\frac{h}{\sqrt{N_p}\, k_f} = \text{Const.} \left[\left(\frac{\Delta T_{sat}\, \rho_f\, C_{pf} \sqrt{a_f}}{\rho_g\, i_{fg}} \right)^2 \frac{1}{\nu_f} \right]^m \left(\frac{\nu_f}{a_f} \right)^n (D_d \sqrt{N_p})^p \tag{54}$$

where D_d can be calculated from Eq. (47).

Fitting the available experimental data with the proposed equation, Eq. (54) resulted in the following correlation

$$\frac{h}{\sqrt{N_p}\, k_f} = 14.0 \left[\left(\frac{\rho_f}{\rho_g} \right) \left(\frac{C_{pf}\, \Delta T_{sat}}{i_{fg}} \right) \right]^{0.5} \left(\frac{\nu_f}{a_f} \right)^{-0.39} (D_d \sqrt{N_p})^{-0.25} \tag{55}$$

which can be expressed in dimensional form as follows

$$h = 14.0 \left(\frac{\rho_f\, C_{pf}}{\rho_g\, i_{fg}} \right)^{0.5} \left(\frac{\nu_f}{a_f} \right)^{-0.39} \frac{k_f}{D_d^{0.25}} (\Delta T_{sat})^{0.5}\, N_p^{0.375} \quad . \tag{56}$$

A comparison of the predicted results with the experimental values is presented in Figs. 7 and 8. Considering the variety of surfaces and fluids used in experiments, Eq. (55) correlates the available experimental data reasonably well over a wide range of variables.

It is interesting to note that the functional relationships between the heat transfer coefficient and the basic characteristic parameters is of the form

$$h \sim (\Delta T_{sat})^{0.5}\, N_p^{0.375} \tag{57}$$

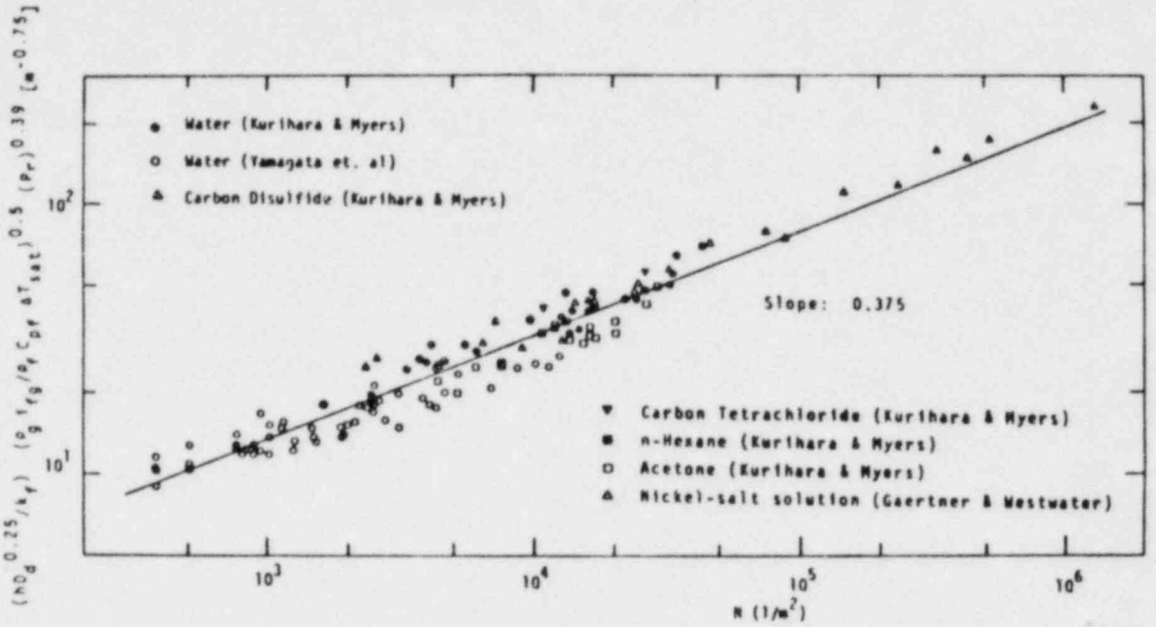

Fig. 7. Correlation of Heat Transfer Coefficient with Active Nucleation Site Density

which is confirmed by the experimental observations, where it was shown [44-50] that the heat transfer coefficient is not a single-valued function of the superheat temperature difference, but depends upon both the superheat and the active nucleation site density.

IV. ACTIVE NUCLEATION SITE DENSITY DISTRIBUTION IN POOL BOILING

A. Surface Effects

An empirical correlation given by Eq. (55), relating the heat transfer coefficient to active nucleation site density N_p, liquid superheat ΔT_{sat}, and the fluid characteristics, offers a method of predicting h in terms of ΔT_{sat} and N_p for various liquids. Through N_p the structure of the heating surface is taken into account. Basically, the active nucleation site density reflects the effects of the surface characteristics on boiling performance. The next phase of the problem, therefore, is to describe the surface nucleation characteristics by correlating the total number of active nucleation sites at certain boiling conditions.

The analysis of Refs. [59] and [60] has indicated that the number of active sites can be determined as a function of wall superheat or heat flux if the distribution of cavities on the surface is known. Unfortunately, so far the distribution of cavities cannot be directly determined by measurements. However, as proposed in Ref. [38] the size density of nucleation sites can be determined by inference from experimental data. The extensive experiment [38], in which the nucleation properties of single artificial cavities were investigated for water, methanol, and ethanol on different copper surfaces finished with emery paper, confirmed the occurrences of nucleation from the

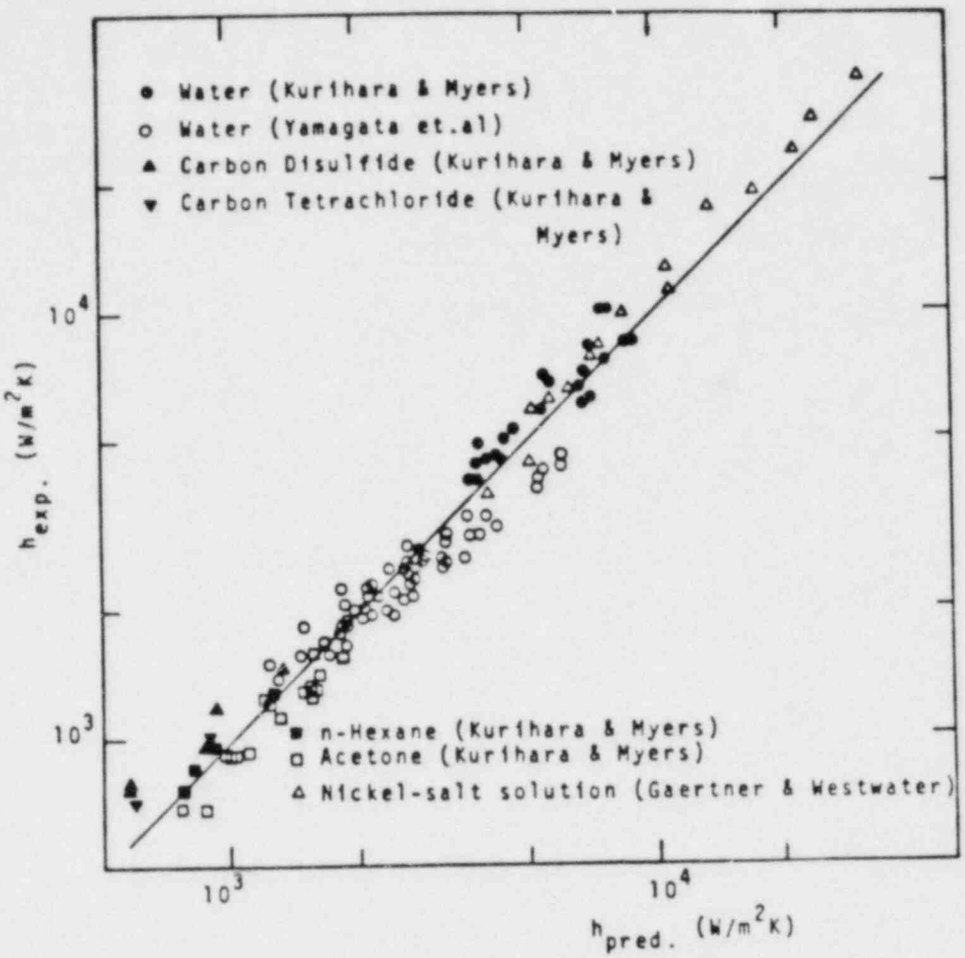

Fig. 8. Comparison of Predicted Heat Transfer Coefficient with Experimental Values

preexisting gas filled cavities on the surface. Furthermore, a simple relation for the critical cavity size given by

$$R_c = \frac{2 \sigma T_{sat}}{\rho_g i_{fg} (T_w - T_{sat})} \tag{58}$$

was found to be sufficient to characterize such an active cavity, since the surface superheat at which a cavity would become active was found to be fixed by the fluid properties through this relationship. For a particular surface, a single plot of active site density N_p versus parameter grouping R_c was obtained at a given pressure. Consequently, it was concluded that the nucleation characteristics of a surface would be known if the size distribution of active sites on the surface were known. Later, this type of approach to the problem was followed by many investigators [47, 61, 65]. However, the validity of such an approach depends upon the correct usage of the relationship between ΔT_{sat} and R_c, that is, the correct choice of incipience boiling criteria. Besides, the method is equivalent to a calibration method. That means

when a new surface is given, a new calibration has to be made; otherwise, there is only a qualitative correlation between surface finish and size range of cavity density.

Furthermore, it should be noted here that the use of Eq. (58) in predicting the critical cavity size on all pressure levels is not correct. As demonstrated in Appendix B, Eq. (58) can give only correct results for water at about 50 bars, see Fig. 9. For lower and higher pressures, the error in calculating R_c increases as the liquid superheat increases. Based on this observation, a more accurate expression for R_c is recommended at extreme pressure ranges.

From this brief discussion it can be concluded that the basic problem to correlate the active site density to the surface nucleation characteristics is due largely to the difficulty of describing the surface effect quantitatively. Until the time when the essential elements of a surface which affects boiling can be measured and are related mathematically to boiling performance, it is unlikely that any truly reliable correlation will be developed.

B. Validity of $N_p - N_p (R_c)$ Relation

As discussed in the preceding section, the essential effects of a boiling surface cannot be measured and related mathematically to an active nucleation site density distribution. Therefore, it is unlikely that any reliable correlation based on mechanistic modeling can be developed for determining N_p. Instead one may proceed with data reduction techniques by means of dimensionless groups.

It may be reasonable to start from the fact that a certain number of properties and variables characterize the process. Such variables and the thermophysical properties are N_p, ΔT_{sat}, D_d, T_{sat} and ρ_f, ρ_g, v_f, a_f, C_{pf}, i_{fg}, σ, respectively. These variables and properties may be combined in the usual way of dimensional analysis to yield dimensionless groups, and the linear or nonlinear regression analysis with the existing data can be used to derive a correlation between dependent and independent dimensionless variables. Considering the number of independent dimensionless groups and the number of substances used in boiling experiments, the method just described would be too cumbersome. Since our purpose is directed toward obtaining an empirical correlation for water only, it seemed reasonable to eliminate some of the variables listed above.

From the list above it can be observed that the main variables affecting on N_p are the liquid superheat, the bubble departure diameter and the thermophysical properties of fluid. Since both the bubble departure diameter, see Appendix A, and the fluid properties may be represented as a function of pressure, it may be proposed that

$$N_p = N_p (\Delta T_{sat}, p) \quad . \tag{59}$$

None of the experimenters, when investigating the effect of pressure on boiling performance, simultaneously counted active nucleation site density, so the validity of the proposed functional relationship given by Eq. (59)

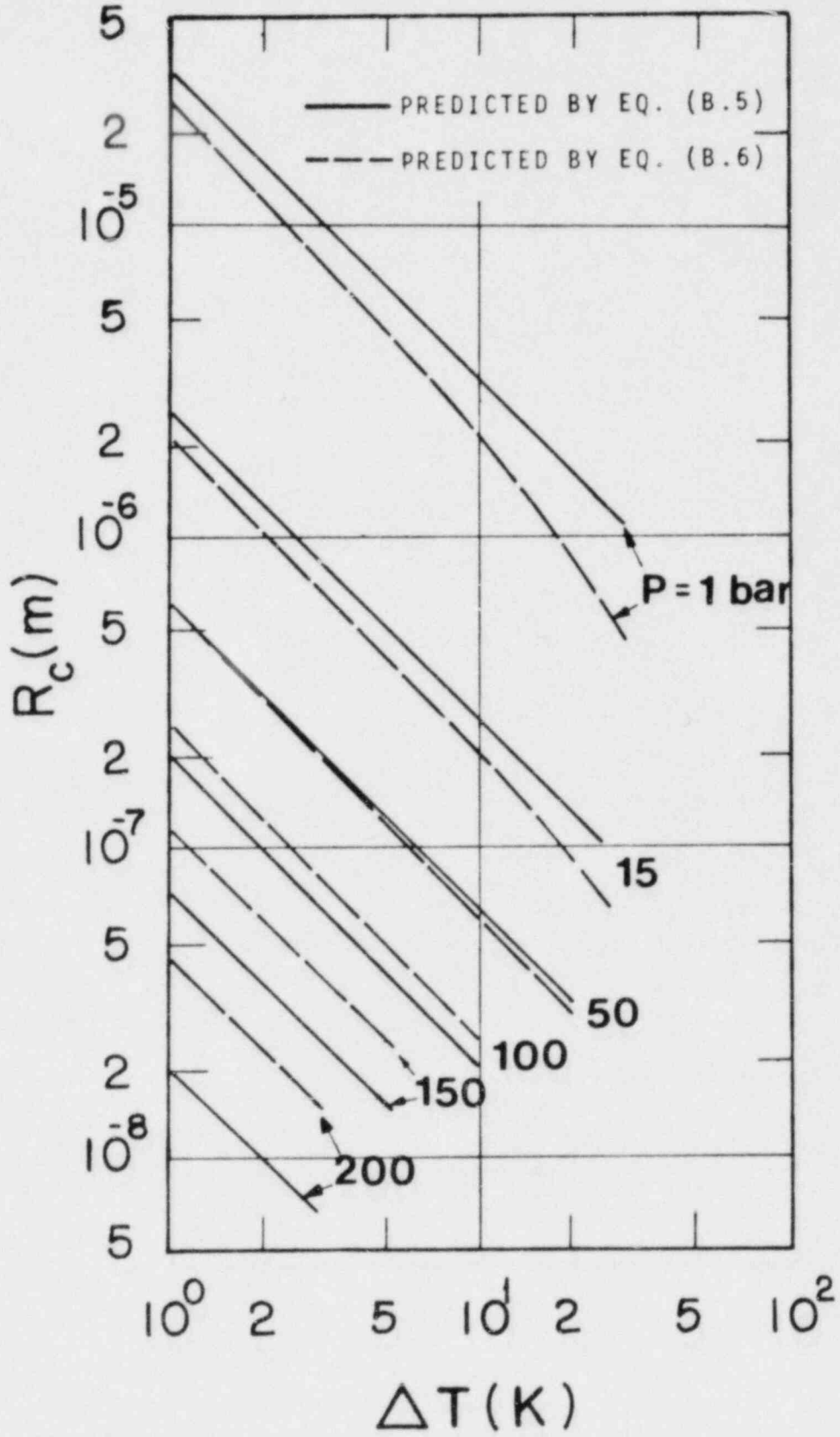

Fig. 9. Relationship of Critical Cavity Size to Liquid Superheat at Different Pressures

cannot be confirmed directly. Instead, the heat transfer correlation developed in the preceding section, i.e., Eq. (55), may be used to calculate the active nucleation site density from experimentally measured values of ΔT_{sat} and h. Applying Eq. (55) to the experimental water data [66], the active nucleation site density versus ΔT_{sat} was plotted in the double logarithmic diagram as shown in Fig. 10. It can be seen from this figure that a relation in the form of

$$N_p = \text{Const.}\ \Delta T_{sat}^m \tag{60}$$

exists at a given pressure level. However, the constant term appearing in Eq. (60) exhibits drastic variations from one pressure level to another pressure level.

Equation (60) can also be expressed in nondimensional form by using proper scaling parameters for N_p and ΔT_{sat}. A natural scaling parameter for N_p should be the bubble departure diameter, D_d, because in maximum packing condition

$$N_p\ D_d^2 \leq 1.0\ . \tag{61}$$

Thus, the dimensionless active nucleation site density is defined as

$$N_p^* = N_p\ D_d^2\ . \tag{62}$$

On the other hand, the proper scaling parameter for ΔT_{sat} might be the maximum possible value of the liquid superheat at a given pressure. However, in view of the difficulties associated with predicting the maximum superheat, we used the nondimensional critical cavity size, R_c, because R_c reflects the effect of superheat at a given pressure. Furthermore, it should be noted that the critical radius calculated from Eq. (B.5), or more correctly from Eq. (B.6), is equal to the minimum cavity size that can be activated at a given superheat ΔT_{sat}, while the active nucleation site density N_p at given ΔT_{sat} and P comprises all nucleation sites with cavity radii $r \geq R_c$. Thus, calculating N_p and R_c for different values of ΔT_{sat} and p and plotting N_p against R_c, one obtains the cumulative size distribution. With the minimum radius calculated by Eq. (41), values of N_p versus dimensionless minimum radius defined by

$$R_c^* = \frac{R_c}{D_d/2} \tag{63}$$

were plotted in Fig. 11. It can be seen from this figure that a relation in the form of

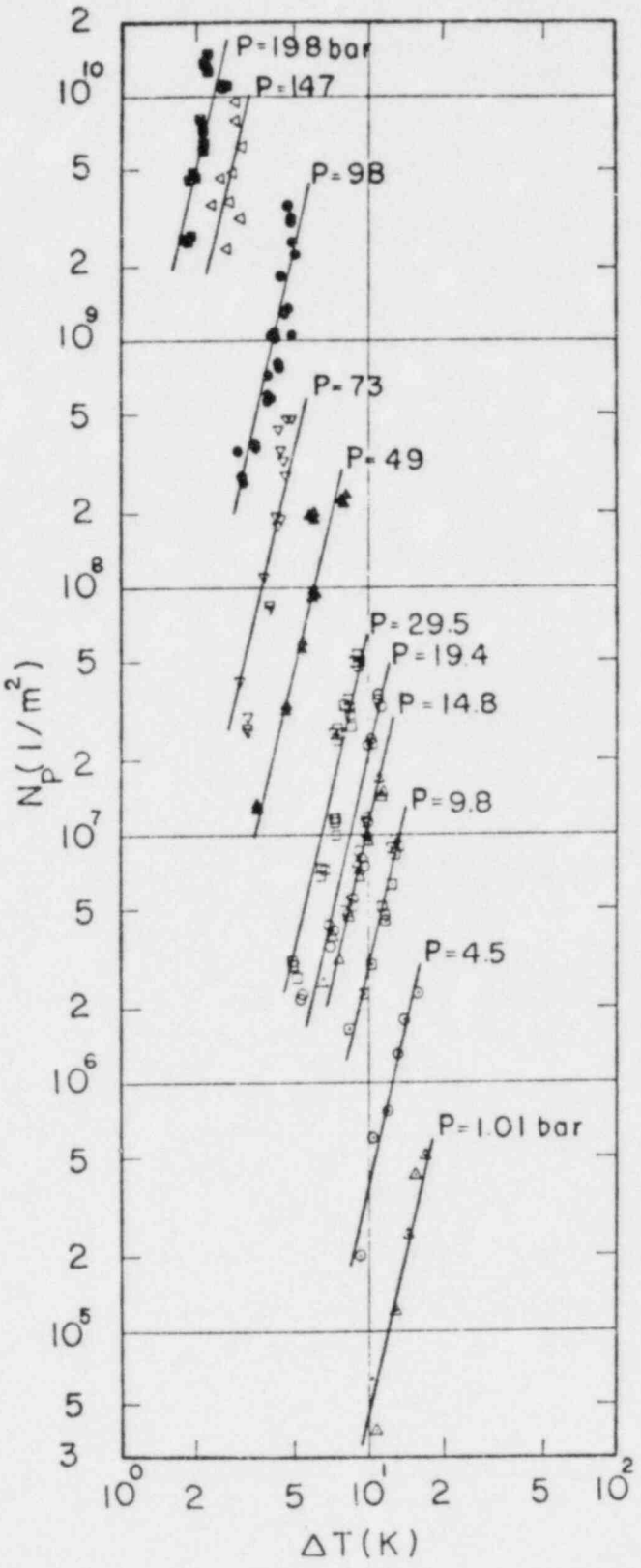

Fig. 10. Active Nucleation Site Density vs. Liquid Superheat at Different Pressures [66]

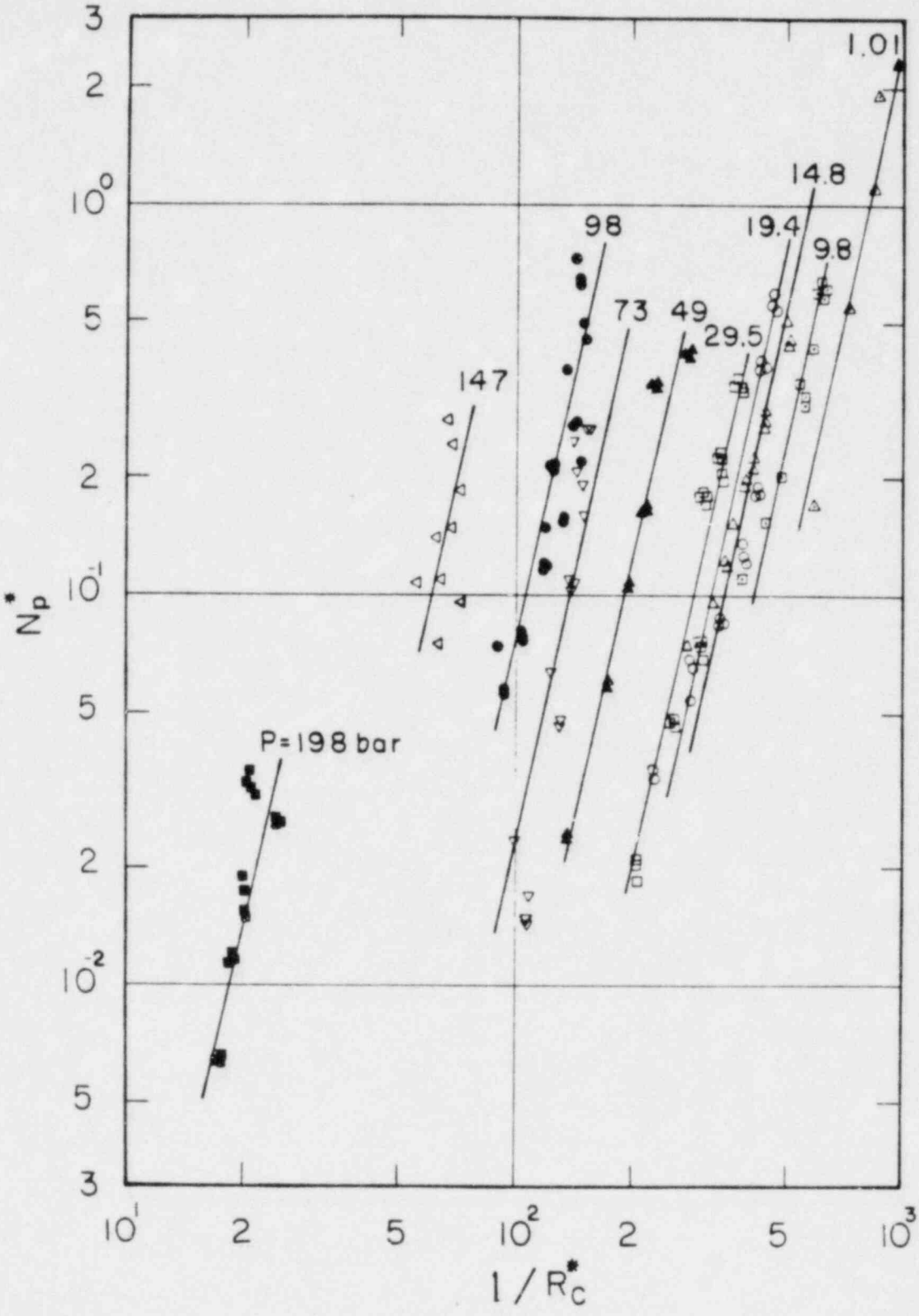

Fig. 11. Dimensionless Active Nucleation Site Density vs. Dimensionless Critical Cavity Size at Different Pressures [66]

$$N_p^* = \text{Const.}\ R_c^{*n} \tag{64}$$

at each pressure level confirms the validity of an approach followed by Refs. [47] and [61-65] based on the above equation. However, to the contrary of the findings in these references, the constant term appearing in Eq. (64) strongly depends on the system pressure.

This parametric investigation supports a functional relationship of the type proposed by Eq. (59). Furthermore, it conclusively shows that the active nucleation site density is not a single-valued function of the critical radius, R_c, but depends upon both the critical radius and the saturation pressure. This final conclusion contradicts the conclusions obtained in Refs. [47] and [61-65]. Contradictions stem from the fact that variations in R_c in these experiments were achieved by varying the superheat alone at a single system pressure.

C. Global Correlation

In order to establish both the pressure and the surface effects, which cannot be accounted for by a correlation in the form of either Eq. (60) or Eq. (64), a global approach to the problem was followed in the present investigation. Namely, the heat transfer correlation expressed by Eq. (55) was used with the experimental data run on a variety of sufaces to correlate the active nucleation site density to measureable quantities. This overall approach certainly eliminates the detailed effects of the surface characteristics on the nucleation site density. However, it will take into account the surface characteristics on averaged or global sense.

In view of the parametric study made in the preceding section, it was sought to arrive at a correlation in the form of

$$N_p^* = R_c^{*m}\, f(\rho^*) \tag{65}$$

where ρ^* is the nondimensional density difference given by

$$\rho^* \equiv \Delta\rho/\rho_g \quad . \tag{66}$$

Applying Eq. (55) to the existing water data listed in Table II, N_p was calculated from experimentally measured values of ΔT_{sat} and h while Eq. (B.6) were used to evaluate R_c. Fitting the data with Eq. (65) exponent m and function $f(\rho^*)$ were determined. The results can be represented as

$$N_p^* = f(\rho^*)\ R_c^{*-4.4} \tag{67}$$

where

Table II. Pool Boiling Heat Transfer Experimental Data

Author(s) [Reference]	Geometry	Heater Size (Diameter) (cm)	Material roughness	Pressure (bar)
Borishanskii et al. [66]	Cylinder	D = 0.694 L = 26.0	Stainless Steel 1 x 18 H 9 T	4.51, 73.05, 98.1, 147.1, 196.1
Borishanskii et al. [68]	Cylinder		Stainless Steel 1 Kh 18 N 9 T Clean	5.88, 9.81, 22.6, 31.4, 42.2, 55.0, 99.1, 128.5, 147.0, 169.0, 178.0
Cichelli & Bonilla [67]	Flat Plate	D = 9.5	Chromium Plated Copper, Clean and Polished	7.93, 18.28, 35.48, 52.76, 70.0
Magrini & Nannei [69]	Cylinder	D = 1.0 L = 19.0	Layer of Zinc, Nickel and Tin, Polished with Emery Paper	1.01
Elrod et al. [70]	Cylinder	D = 1.91 t = 0.124 L = 17.78	Carbon Steel Monel and Inconel Commerical Material	36.86, 70.0 106.8

$$f(\rho^*) = 2.157 \times 10^{-7} \left(\frac{\Delta\rho}{\rho_g}\right)^{-3.12} \left(1 + 0.0049 \frac{\Delta\rho}{\rho_g}\right)^{4.13} \quad . \tag{68}$$

A comparison of the above correlation with the experimental data is presented in Fig. 12. Considering the variety of surfaces with different roughnesses used in the experiments, one should notice that Eq. (67) allows a fairly good representation of the existing experimental water data for a pressure range of 1 bar to 198 bars. It should be noted that the correlation expressed by Eq. (67) is a global one because it represents the effects of surface characteristics only on averaged sense.

V. FORCED CONVECTIVE NUCLEATE BOILING

A. Active Nucleation Site Density

In the preceding section, the active nucleation site density in pool boiling is correlated in the form of $N_p^* = N_p^* (R_c^*, \rho^*)$. It is the objective of this section to show that a similar correlation can be used in predicting the active nucleation site density in a forced convection system.

In forced convective nucleate boiling, which covers the fully developed subcooled boiling and the saturated nucleate boiling regions, Fig. 2, the velocity and subcooling have only little effect [53, 54] on the surface temperature. It was shown that the wall temperature strongly influences the active nucleation site density in the pool boiling. In subcooled boiling, the surface temperature is primarily a function of the surface heat flux and the system pressure for a given fluid. Since the saturation temperature depends on the system pressure only, it may seem that the flow field would not be effective on the overall wall superheat. However, in view of the following discussion it will be clear that the hydrodynamic flow field will have a significant effect on the effective superheat in which a bubble grows in convective nucleate boiling.

A bubble nucleated at a cavity grows through a liquid film region adjacent to the wall where a high temperature gradient exists, and so in reality it experiences a somewhat lower mean superheat than the wall superheat. In the case of pool boiling the difference between the wall superheat and the actual superheat that a growing bubble experiences is small. Therefore, the superheat based on the surface temperature, T_w, can be taken as the effective superheat in pool boiling. In the case of forced convective nucleate boiling, however, the temperature gradient depends on the mass flow rate and would generally be much steeper than in the corresponding pool boiling case with the same wall superheat. However, the effective superheat would be less than the actual wall superheat. Qualitative temperature profiles for pool boiling and for convective boiling with the same actual wall superheat is presented in Fig. 13. From this figure it can be seen that

$$\Delta T_{e,\,conv} < \Delta T_{e,\,pool} \simeq \Delta T_{sat} \equiv T_w - T_{sat} \quad . \tag{69}$$

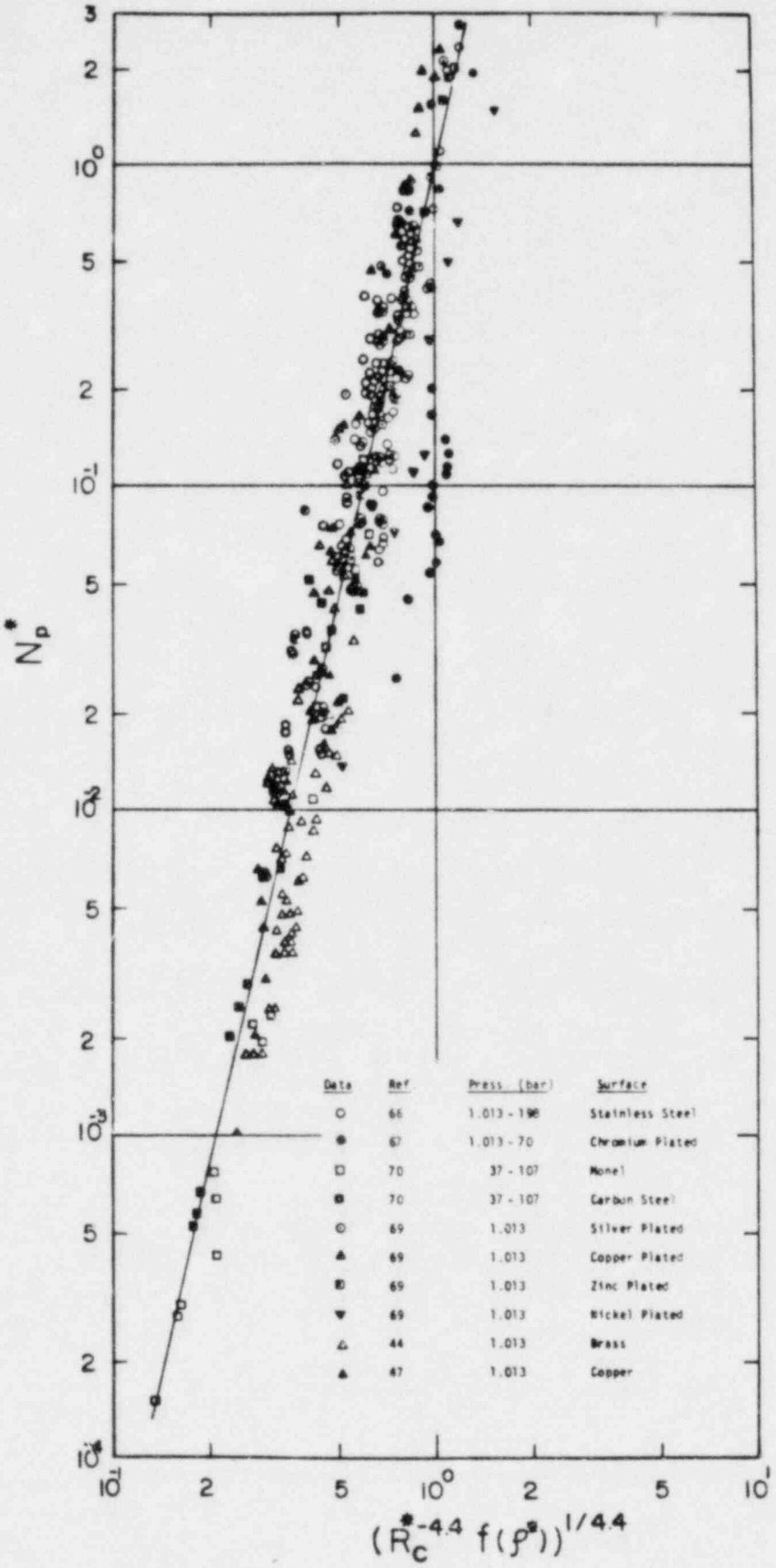

Fig. 12. Correlation of Active Nucleation Site Density in Pool Boiling

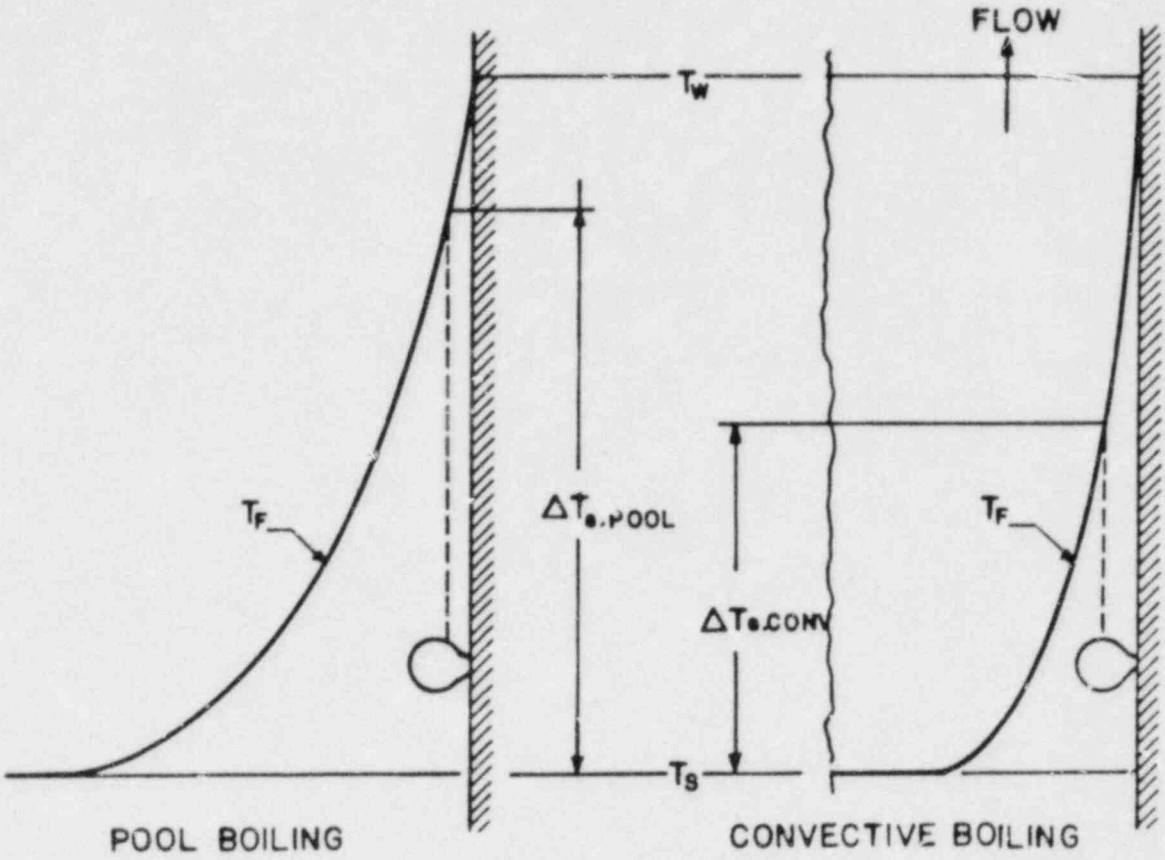

Fig. 13. Temperature Profiles for Pool Boiling and for Convective Boiling with Same Total Superheat [71]

Thus in the forced convective nucleate boiling region, effects of the flow on the nucleation characteristics would be through the temperature gradient rather than the overall wall superheat.

In a mechanistic sense, bubble nucleation process is similar in pool boiling and convective nucleate boiling. In both cases, to maintain nucleate boiling on a surface, it is necessary that the effective superheat exceeds a critical value for a specified system pressure. Thus it is postulated here that the active nucleation site density correlation obtained for the pool boiling could be used to predict the active nucleation site density in a forced convective nucleate boiling with an effective superheat, ΔT_e, rather than the actual wall superheat, ΔT_{sat}. Based on this assumption the active nucleation site density for forced convective nucleate boiling N_a in a dimensionless form is given by

$$N_a^* = N_p^* \left(R_{ce}^*, \rho^*\right) \quad . \tag{70}$$

The effective critical cavity size, R_{ce}, is derived in Appendix B and given by

$$R_{ce} = \frac{2\sigma}{p_f}\left(1 + \frac{\rho_g}{\rho_f}\right) \Bigg/ \left\{ \exp\left[\frac{(T_g - T_{sat})\, i_{fg}}{R\, T_{sat}\, T_g}\right] - 1 \right\} . \qquad (71)$$

In view of Eq. (67), the dimensionless active nucleation site density in the forced convective nucleate boiling can be given by

$$N_a^* = f(\rho^*)\, Re_{ce}^{*-4.4} \qquad (72)$$

where $f(\rho^*)$ is given by Eq. (68).

Based on Eq. (72), the following observations can be made:

1. Since the effective superheat decreases with increasing flow rate, the number of the active nucleation site density decreases with increasing flow rate. This result has been confirmed by experimental observations. At relatively high flow rates the nucleation may be completely suppressed.

2. The number of active nucleation sites increases with increasing surface heat flux. This result is an expected one, because as the total heat flux increases total wall superheat and, in turn, the effective superheat increases, indicating that more and more nucleation sites are activated.

3. Finally, the number of active nucleation sites increases with increasing system pressure. As the pressure increases, Eq. (72) reveals that more nucleation centers are activated.

These immediate results enumerated above support the method developed in this report to predict the active nucleation site density in terms of the fluid and flow parameters.

B. Effective Superheat

A formal way of predicting the effective superheat requires information about the thermal boundary layer profile in the vicinity of the heated surface and the cavity size distribution. For a simplicity of the model, the suppression factor [71] will be introduced here. In Chen's heat transfer correlation [71], which has been proved to be reliable, suppression factor S is defined by

$$S \doteq \left(\frac{\Delta T_e}{\Delta T_{sat}}\right)^{0.99} . \qquad (73)$$

From experimental data it was graphically correlated to a two-phase flow Reynolds number defined by

$$Re_{TP} = [G(1 - x)D/\mu_f] \cdot F^{1.25} \quad . \tag{74}$$

Functional relationships which fit Chen's correlations for F and S respectively are

$$F = 1.0 \text{ for } \frac{1}{X_{tt}} \leq 0.1 \tag{75}$$

$$F = 2.35\left(\frac{1}{X_{tt}} + 0.213\right)^{0.736} \text{ for } \frac{1}{X_{tt}} > 0.1 \tag{76}$$

and

$$S = \frac{1}{1 + 1.4 \times 10^{-5} Re_{TP}} \tag{77}$$

where X_{tt} is the Martinelli parameter [72].

For simplicity the power 0.99 in Eq. (73) may be replaced by 1.0, then the effective superheat can be calculated from

$$\Delta T_e = S \cdot \Delta T_{sat} \quad . \tag{78}$$

C. Comparison

In the case of forced convective nucleate boiling, so far there are almost no experimental data which can provide direct information on the active nucleation site density, except that of Treshchev [86]. The test section in that study was a rectangular duct 8 × 14 mm in size, with a boiling surface of a nickel plate fastened to the bottom. The fluid used in the experiments was water. The heat fluxes ranged from 0.4×10^6 to 5×10^6 W/m^2 and the flow velocities were up to 2 m/s. The number of active nucleation sites was determined by macrophotography, for pressures of 5, 25 and 50 bars and for temperatures from 80 to 250°C. The active nucleation site density, N_p, was observed as a function of the surface heat flux, $\dot{q}$". System pressure, liquid velocity and the liquid subcooling were treated as parameters.

Since the surface temperature was not simultaneously measured in Treshchev's experimental study, it was not possible to make a direct comparison with the present correlation. For the purpose of comparison, however, the surface temperatures were calculated from the correlations of Chen [71] and Thom [74]. Since the liquid subcoolings in these experiments were as high as 85°C, properties used in the calculation of the Reynolds number are based on the liquid bulk temperature. However, the actual wall superheats in the forced convective nucleate boiling are much higher than the superheats encountered in the pool boiling. Thus the properties relevant to bubble formation are determined

at the average film temperature. With the wall temperatures calculated from the Chen and Thom's correlations, dimensional active nucleation site densities predicted by Eq. (72) are compared with Treshchev's experimental observations in Figs. 14 and 15. In order to cover the whole range of experimental parameters, a comparison is made in Fig. 16 in terms of dimensionless variables. Considering the detailed surface effects which were not taken into account in our correlation, it can be seen from these figures that the active nucleation site density predicted by Eq. (72) allows a fairly good representation of the only existing experimental water data for a pressure range of 1 to 50 bars. In particular, wall temperatures based on Chen's correlation yield better results than that based on Thom's correlation.

D. Use of Simple R_c Relation

As demonstrated in Appendix B, use of a simple expression, i.e., Eq. (B.5), for the critical cavity size may yield erroneous results at certain system pressures. For this reason, the complete expression given by Eq. (B.6) has been used throughout in this report. Due to its simplicity, however, the simple expression has been consistently used in the literature. It is inversely proportional to the liquid superheat, and, therefore, it can be considered as a representative of liquid superheat. Defining a dimensionless superheat by

$$T^* = \left(\frac{R_c}{D_d/2}\right)^{-1} = \frac{\rho_g \, i_{fg} \, (T_g - T_{sat})}{\sigma \, T_{sat} \, p} \tag{79}$$

it is interesting to see how the use of Eq. (79) represents the pool boiling and convective nucleate boiling data.

In view of Eq. (79), the pool boiling correlation, i.e., Eq. (67) can be recast in the following form

$$N_p^* = \Delta T^{*4.4} \, f(\rho^*) \tag{80}$$

whereas the convective nucleate boiling correlation given by Eq. (72) can be expressed as

$$N_a^* = \Delta T_e^{*4.4} \, f(\rho^*) \tag{81}$$

where $f(\rho^*)$ is defined by Eq. (68). Based on these correlations, similar figures to Fig. 12 and Fig. 16 are generated in Figs. 17 and 18, respectively. It can be seen from these figures that there exists a qualitative agreement between the calculated and the experimentally observed data points. However, discrepancy is increased in a quantitative sense if we compare Fig. 12 with Fig. 17 and Fig. 16 with Fig. 18. Relatively good agreement between Figs. 16 and 18 is due to low pressures used in experiments. Source of error can be explained by examining Fig. 9, where predicted values of R_c based on Eq. (B.5)

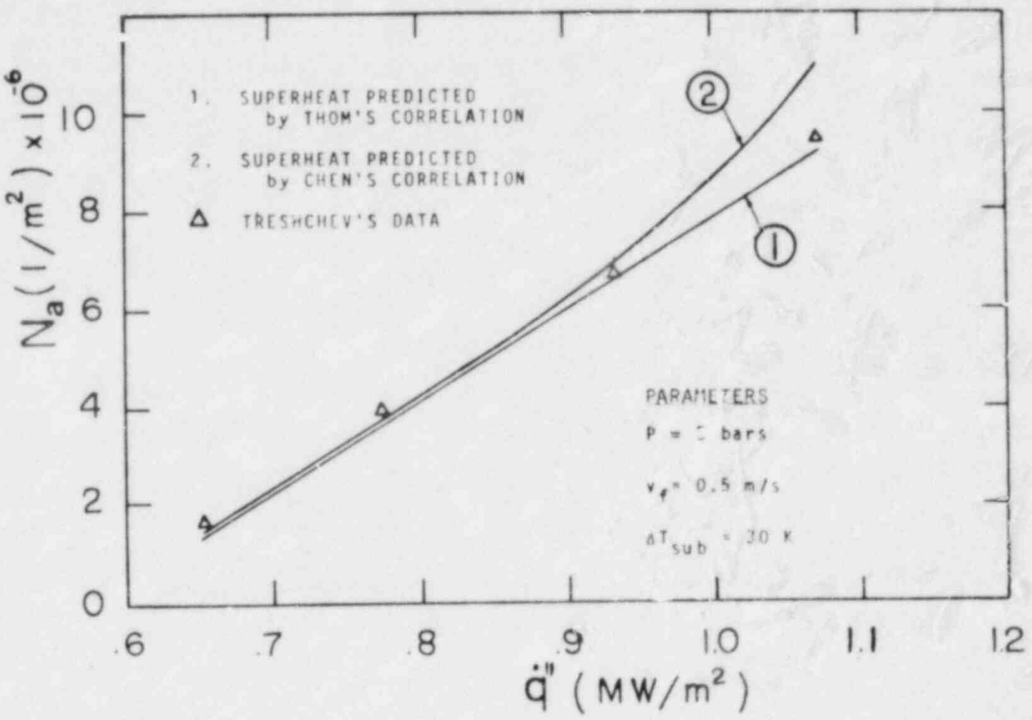

Fig. 14. Comparison of Calculated Active Nucleation Site Density with G. G. Treshchev's Convective Boiling Data [86]

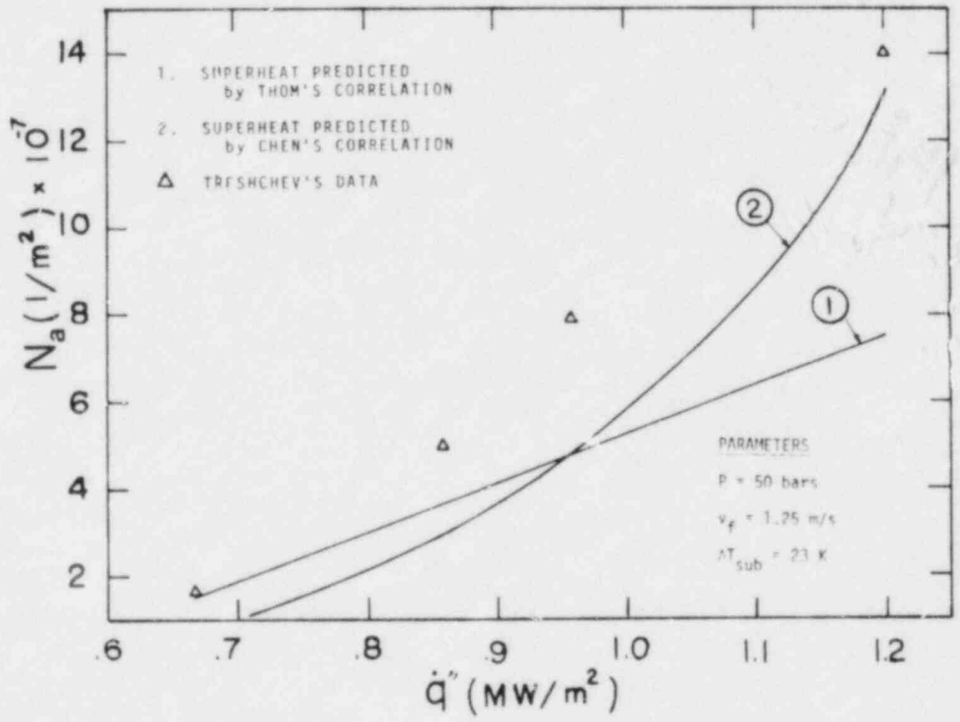

Fig. 15. Comparison of Calculated Active Nucleation Site Density with G. G. Treshchev's Convective Boiling Data [86]

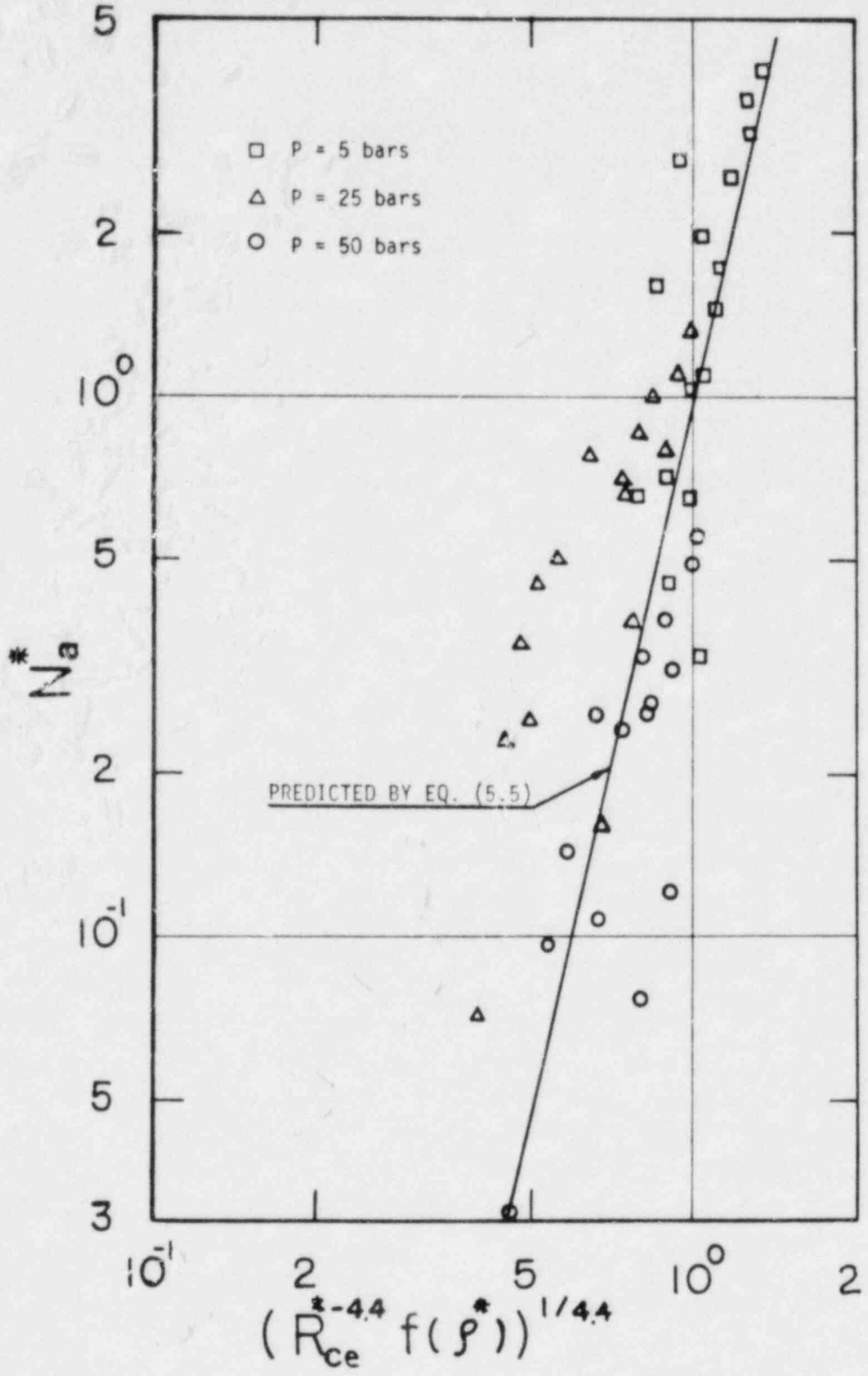

Fig. 16. Comparison of Calculated Dimensionless Active Nucleation Site Density with Experimental Convective Boiling Data [86]

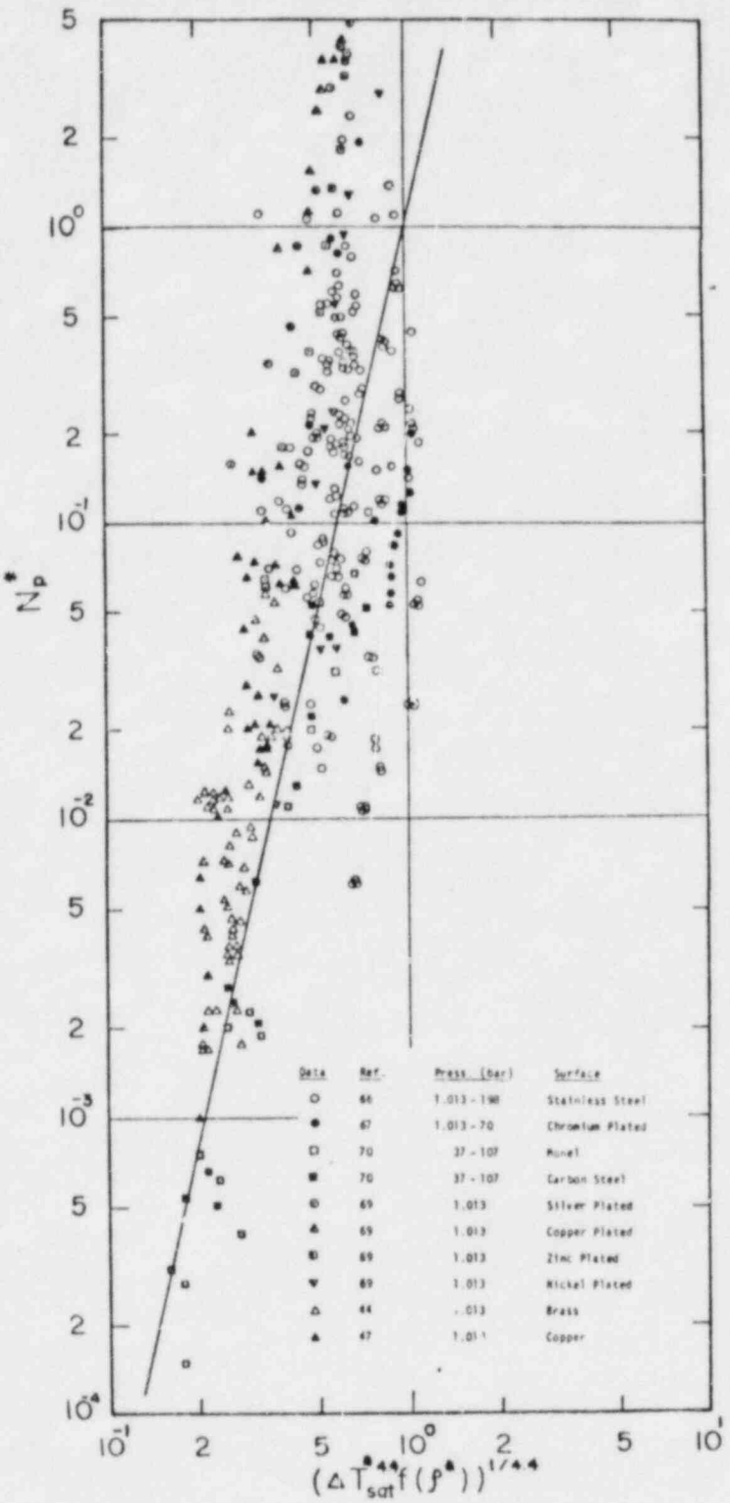

Fig. 17. Use of Simple R_c Relation in Pool Boiling Correlation

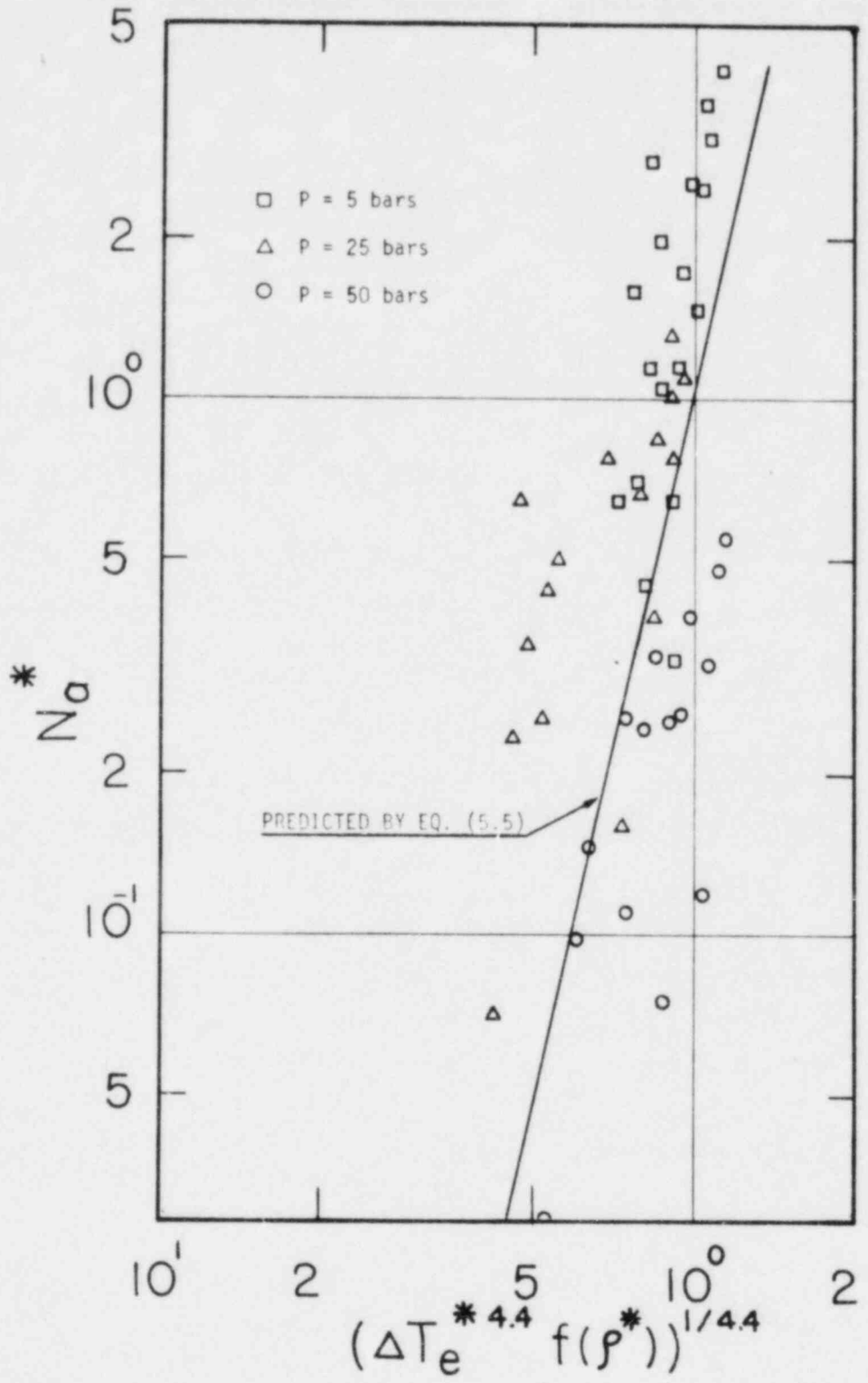

Fig. 18. Use of Simple R_{ce} Relation in Convective Nucleate Boiling

and Eq. (B.6) are compared. It can be seen from this figure that the simple relation yields relatively good values for R_c around 50 bars pressure. Discrepancy between Eq. (B.5) and Eq. (B.6) increases when the system pressure is far from 50 bars. From this brief comparison, it can be concluded that the simple expression for the critical cavity size may be acceptable for a system pressure in the range of 25 to 100 ata.

VI. SUMMARY AND CONCLUSIONS

Among the macroscopic parameters, void fraction, shape factor and the bubble number density, which affect the interfacial area concentration in the bubbly two-phase flow system, the bubble number density is formulated in terms of the number density differential balance equation. It is shown that the bubble number density is related to the homogeneous and heterogeneous bulk liquid nucleation, the wall cavity nucleation and the bubble recondensation rates through the source and sink terms appearing in the differential equation. Based on the formation mechanisms of bubbles from different sources, it is concluded that: 1) for water at least, the homogeneous nucleation can be discounted as a mechanism of bubble generation, 2) the heterogeneous nucleation in the bulk liquid can be significant in a flow channel with rapid depressurization, 3) in a practical system with heat addition, bubble nucleations at the external boundaries and the bubble collapse due to recondensation in the subcooled bulk liquid become more important than the bulk nucleation. As a first step, therefore, the active nucleation site density at external boundaries and the bubble collapse rate variations with fluid and flow parameters are studied in detail in this report.

Based on the overall energy and mass balance equations, the bubble sink term, that is the bubble recondensation rate, is formulated in terms of cavity nucleation rate and the liquid bulk temperature gradient. Furthermore, using the existing correlation for the temperature profile, the sink term is expressed in terms of the liquid temperature differences and the wall nucleation rate.

Starting from the fact that there exists mechanistic similarity in cavity nucleation between the pool boiling and the convective nucleate boiling, active nucleation site density studies are carried out for pool boiling. Although a number of pool boiling data providing quantitative information on the active nucleation site density have been accumulated over the years, none of the experimenters when investigating the effect of pressure on boiling performance simultaneously counted active nucleation site density. Most of the existing data have been obtained at subatmospheric pressures. Almost no data exist for higher system pressures beyond 1 atm.

In view of the above, pool boiling heat transfer coefficient is correlated to the liquid superheat and the active nucleation site density based on the growing bubble agitation model. Then, this heat transfer correlation is used to calculate the active nucleation site density from experimentally measured values of liquid superheats and heat transfer coefficients for a wide range of system pressure covering 1 bar to 198 bars, and the dimensionless active nucleation site density is correlated to the dimensionless cavity size and the density ratio. This finding has conclusively shown that the active nucleation site density depends upon both the critical radius and the saturation pressure.

It must be noted here that this correlation takes into account the surface effects in an averaged sense, because experimental data used in the development of the correlation are obtained from different sources with a variety of boiling materials and surfaces.

In view of the mechanistic similarity in bubble nucleation, it is postulated that the pool boiling active nucleation site density correlation could be used to predict the active nucleation site density in the forced convective nucleate boiling wtih an effective liquid superheat rather than the actual wall superheat. Furthermore, using Chen's suppression factor in predicting the effective superheat, a method was developed to determine the nucleation site density. The method offered in this report permits a simple and rapid evaluation of the active site density in terms of the basic fluid and flow parameters in convective nucleate boiling.

The method is tested against the only subcooled nucleate boiling experimental data available in the literature. The good qualitative as well as quantitative agreement between experimentally measured active nucleation site density and those calculated by the method offered in this report appears to verify the basic principles involved in the development.

APPENDIX A

Bubble Departure Diameter

The earliest relation for the departure diameter of a bubble is based on a balance of buoyancy force against the surface tension and was given by Fritz [58] in 1935. The equation proposed by Fritz is

$$D_{dF} = 0.0208\ \theta \left(\frac{\sigma}{g\Delta\rho}\right)^{1/2} \qquad (A.1)$$

where θ is the contact angle measured in degrees.

Following this early study many other papers have been published on this problem [40, 60, 76-85]. The validity of semi-theoretical predictions of the bubble departure diameter and, in turn, of active nucleation site density distribution and heat transfer correlations, however, is limited, because there seems insufficient bubble departure diameter data available. A list of previously published experimental data given in Ref. [83] shows that most of the existing data have been obtained at subatmospheric pressures. In addition, only a very small number of bubbles have been evaluated. Due to the well-known scatter of bubble nucleation and formation, further experiments are needed.

Based on the available experimental water data, an effort has been made in this investigation to obtain an empirical expression for the bubble departure diameter, which can be used at different pressure levels much higher than atmospheric pressure.

Hatton and Hall [78] in their detailed study of the bubble departure diameter concluded that bubble departure diameter is relatively independent of heat flux but strongly depends on cavity size, R_c, and pressure. Since the active cavity size is inversely dependent on the superheat and the system pressure, it can be tentatively stated that key parameters affecting the departing bubble size are the superheat temperature difference and pressure. However, the latest experimental data [85], which covered pressure range of 1.1 bars to 8.0 bars, indicates that the departure diameter decreases as the superheat increases at 1.1 bars, and it is almost independent of temperature difference at higher pressures. This observation coincides very well with the experimental results obtained in Ref. [81].

The same trend, that departing bubble diameter is a very strong function of pressure alone, was found empirically by Nishikawa and Urakawa [76] as

$$D_d = 0.0037/P^{0.575} \qquad (A.2)$$

and by Semeria [40] as

$$D_d = 0.0016/P^{0.5} \qquad (A.3)$$

where D_d is in meters and P is in bars.

In view of the above discussion it is possible to state that, for water at least, the bubble departure diameters are independent of the superheat at a relatively higher pressure, but they are very strong functions of pressure. In fact the departure diameter decreases as pressure increases.

In order to arrive at a simple empirical relation between D_d and p, existing data for bubble departure diameter of water as a function of $\Delta\rho/\rho_g$ is illustrated in Fig. 6. For the purpose of comparison, equations proposed in Refs. [40], [58] and [76] are also plotted in the same figure. It should be noted that Tolubinsky and Ostrovsky's convective boiling experimental data, [81], are also included in the figure, because it is thought that both pool and convective nucleate boiling processes are similar in terms of local agitating processes. It can be seen from this figure that the Fritz's equation represents the data around atmospheric pressure very well; however, at higher pressures it overestimates the bubble departure diameter. This may be due to the fact that buoyancy and surface forces, upon which the Fritz's equation is based, prevail only in quasistatic bubble growth. At higher pressures smaller cavities are activated. Therefore, the dynamic forces, such as inertia and drag, must be included in addition to static forces.

Since the Fritz's equation has been used more often than any other expression, and since it represents the data very well around 1 atm pressure, it is modified to fit the experimental data in averaged sense. The modified Fritz's equation obtained in this way is given by

$$D_d = 2.5 \times 10^{-5} \left(\frac{\Delta\rho}{\rho_g}\right)^{0.9} \theta \left(\frac{\sigma}{g\Delta\rho}\right)^{1/2} . \qquad (A.4)$$

D_d calculated by Eq. (A.4) reduces to the Fritz's equation as the pressure approaches to atmospheric pressure. At the present, the maximum systems pressure at which the bubble departure diameters in water have been investigated equals to 20 bars. For higher pressures the results are extrapolated due to the fact that D_d must approach to zero as pressure approaches to the critical pressure, that is as $(\Delta\rho/\rho_g)$ approaches to zero.

It should be noted that the bubble departure diameter equation expressed by Eq. (A.4) does not yet include the effects of all relevant properties of surface material and boiling fluid. More research may be needed to achieve this objective. However, the results reported here seem to justify the very strong dependence of the bubble departure diameter on the system pressure.

APPENDIX B

Critical Cavity Size

Since the active nucleation site density, N_p, primarily represents the surface characteristics, the critical cavity size, R_c, has become part of the active nucleation site density correlations. From the mathematical point of view, different functional representations, such as power functions and exponential functions, have been proposed. In this report it is shown in Section IV-C that

$$N_p^* \sim R_c^{*-4.4} \quad . \tag{B.1}$$

Considering the numerical value of the exponent appearing in Eq. (B.1), it can be concluded that the validity of theoretical predictions of the active nucleation site density is limited by the expressions used for the theoretical evaluation of R_c.

The accurate relationship for the superheat $(T_g - T_{sat})$, which is required to keep a bubble of radius R_c in unstable equilibrium, is given in Ref. [87] by

$$T_g - T_{sat} = \frac{R\, T_g\, T_{sat}}{i_{fg}} \ln \left[1 + \frac{2\sigma}{p_f\, R_c} \left(1 + \frac{\rho_g}{\rho_f} \right) \right] \quad . \tag{B.2}$$

If $\rho_g << \rho_f$ and $(2\sigma/P_f R_c) << 1$, then Eq. (B.2) simplifies to

$$T_g - T_{sat} = \left(\frac{2\sigma\, T_{sat}}{R_c\, i_{fg}} \right) \left(\frac{R\, T_g}{p_f} \right). \tag{B.3}$$

To simplify further, use can be made of the perfect gas law

$$T_g - T_{sat} = \frac{2\sigma\, T_{sat}}{\rho_g\, i_{fg}\, R_c} \tag{B.4}$$

which can be used to evaluate R_c as follows

$$R_c = \frac{2\sigma\, T_{sat}}{\rho_g\, i_{fg}\, (T_g - T_{sat})} \quad . \tag{B.5}$$

Due to its simplicity, Eq. (B.5) has been consistently used in the literature to evaluate R_c.

For the purpose of comparison, Eq. (B.2) is recast in the following form

$$R_c = \frac{2\sigma}{\rho_f}\left(1 + \frac{\rho_g}{\rho_f}\right) \Bigg/ \left\{ \exp\left[\frac{(T_g - T_{sat})i_{fg}}{R\,T_g\,T_{sat}}\right] - 1 \right\} \qquad (B.6)$$

and the values for R_c predicted for water using Eqs. (B.5) and (B.6) are presented in Fig. (9), where pressure is treated as a parameter. It can be seen from this figure that the behavior of these two equations is rather strange. In the relatively low pressure region, $P \leq 50$ bars, the simple expression given in Eq. (B.5) overestimates the critical cavity size, and the difference increases as the liquid superheat increases. However, at higher pressures, $P > 50$ bars, behavior changes, and the simple relation underestimates the critical cavity size. Again, difference in R_c increases as the system pressure increases.

Since N_p is proportional to -4.4 power of R_c, a small error made in predicting R_c leads to a significant error in the value of N_p. Error becomes much more significant for liquid metals. In order to reduce the error in this report, R_c is evaluated by Eq. (B.6).

ACKNOWLEDGMENTS

The authors would like to express their appreciation to Dr. N. Zuber of NRC for valuable discussions on the subject. This work was performed under the auspices of the U. S. Nuclear Regulatory Commission.

REFERENCES

1. Ishii, M., Thermo-Fluid Dynamic Theory of Two-Phase Flow, Eyrolles, Paris (1975).

2. Delhaye, J. M., "Equations Fondamentales des E'coulements Diphasiques, Part 1 and 2," CEA-R-3429, France (1968).

3. Vernier, P. and Delhaye, J. M., "General Two-Phase Flow Equations Applied to the Thermodynamics of Boiling Nuclear Reactor," Energ. Prim., 4(1) (1968).

4. Boure', J. and Reocrues, M., "General Equations of Two-Phase Flows," 4th All Union Heat and Mass Transfer Conference, Minsk, USSR (1972).

5. Kocamustafaogullari, G., "Thermo-Fluid Dynamics of Separated Two-Phase Flow," Ph.D. Thesis, School of Mechanical Engineering, Georgia Institute of Technology, Georgia (1971).

6. Chawla, T. C. and Ishii, M., "Two-Fluid Model of Two-Phase Flow in a Pin Bundle of a Nuclear Reactor," ANL/RAS/LWR 79-5 (1979).

7. Amsden, A. A. and Harlow, F. H., "K-TIF: A Two-Fluid Computer Program for Downcomer Flow Dynamics," LA-6994, NRC-4 (1978).

8. Thurgood, M. J., et al., "Core Thermal Model Development," PNL-2653-2, NUREG/CR0341, p. 101 (1978).

9. Ishii, M. and Mishima, K., "Two-Fluid Model and Analysis of Interfacial Area," ANL/RAS/LWR 80-3 (1980).

10. Feller, W., An Introduction to Probability Theory and Its Applications, 2nd ed. pp. 215-222, John Wiley and Sons, Inc. New York (1967).

11. Volmer, M., "Kinetik der Phasenbildung," Steinhopf, Leipzig; Edward Bros., Ann Arbor (1945).

12. Knapp, R. T., "Cavitation and Nuclei," Trans. ASME, 80, p. 131 (1958).

13. Simoneau, R. J., "Depressurization and Two-Phase Flow of Water Containing High Levels of Dissolved Nitrogen Gas," NASA Technical Paper 1839 (1981).

14. Clark, Y. P. and Snyder, N. W., "Heat Transfer in Saturated Boiling," Chemical Engineering Progress Symposium Series, 56, No. 30, pp. 25-38 (1960).

15. Griffith, P., Clark, J. A. and Rohsenow, W. M., ASME Paper Number 58-HT-19 (1959).

16. Bowring, R. W., "Physical Model, Based on Bubble Detachment, and Calculation of Steam Voidage in the Subcooled Region of a Heated Channel," Report Number HPR-10, Institute for Atomenergi, Halden, Norway (1962).

17. Dix, G. E., "Vapor Void Fractions for Forced Convection with Subcooled Boiling at Low Flow Rates," Ph.D. Thesis, University of California, Berkeley (1971).

18. Levy, S., International Journal of Heat and Mass Transfer, 10, p. 951 (1967).

19. Staub, F. W., Journal of Heat Transfer, Transaction ASME, 90c, p. 151 (1968).

20. Ahmad, S. Y., "Forced Convection Subcooled Boiling - Prediction of the Onset of Bubble Detachment," Atomic Energy of Canada Limited, Chalk River, Ontario, Canada (1969).

21. Ahmad, S. Y., Journal of Heat Transfer, Transaction ASME 92c, p. 595 (1971).

22. Rouhani, S. Z., Journal of Heat Transfer, Transaction ASME, 90c, p. 158 (1968).

23. Rouhani, S. Z. and Axelsson, E., International Journal of Heat and Mass Transfer, 13, p. 383 (1976).

24. Saha, P. and Zuber, N., "Point of Net Vapor Generation and Void Fraction in Subcooled Boiling," 5th Int. Heat Transfer Conf. Tokyo, Paper B 4.7 (1974).

25. Zuber, N., Staub, F. W. and Bijward, G., "Vapor Void Fraction in Subcooled Boiling and Saturated Boiling Systems," Proceedings of the Third International Heat Transfer Conference, 5, p. 24, AIChE, New York (1966).

26. Bijward, G., Staub, F. W. and Zuber, N., "A Program of Two-Phase Flow Investigation," Eleventh Quarterly Report, October-December 1965, General Electric Co., San Jose, California, Report No. GEAP 5967, Euratom Report No. EURAEC 1575.

27. Kroeger, P. G. and Zuber, N., "An Analysis of the Effect of Various Parameters on the Average Void Fractions in Subcooled Boilings," Int. J. Heat Mass Trans., 11, p. 211 (1968).

28. Jacob, M., Heat Transfer Wiley, New York (1949).

29. Kruzhilin, G., "Generalization of Experimental Data on Heat Transfer to Boiling Liquid Under Conditions of Free Convection," Isv. Akad. Nauk. SSSR, Otd. Teh. Nauk., 967 (1948).

30. Rohsenow, W., "A Method of Correlating Heat Transfer Data for Surface Boiling of Liquids," Trans. ASME, 74, 969 (1952).

31. Kutateladze, S. S., "Heat Transfer in the Case of Condensation and Boiling," Mashgi, Moscow (1952).

32. Forster, H. K. and Zuber, N., "Bubble Dynamics and Boiling Heat Transfer," Amer. Inst. Chem. Engrgs., J., 1, 532 (1955).

33. Levy, S., "Generalized Correlation of Boiling Heat Transfer," Trans. ASME J. Heat Transfer, 81, 37 (1959).

34. Forster, H. K. and Grief, R., "Heat Transfer to Boiling Liquid - Mechanism and Correlation," Trans. ASME J. Heat Transfer, 81, 43 (1959).

35. Nishikawa, K. and Yamagata, K., "On the Correlation of Nucleate Boiling Heat Transfer," Int. J. Heat Mass Trans., 1, 219 (1960).

36. Stephan, K. and Abdelsalam, M., "Heat Transfer Correlations for Natural Convection Boiling," Int. J. Heat Mass Trans., 23, pp. 78-87 (1980).

37. Corty, C. and Foust, A. S., "Surface Variables in Nucleate Boiling," Chem. Eng. Prog. Symp., 51, 17, pp. 1-12 (1955).

38. Griffith, P. and Wallis, J. D., "The Role of Surface Conditions in Nucleate Boiling," Chem. Engrg. Progr. Symp. Ser. No. 30, 56, p. 49 (1968).

39. Gaertner, R. F. and Westwater, J. W., "Population of Active Sites in Nucleate Boiling Heat Transfer," Chem. Engrg. Prog. Symp. Ser. 56, 20, pp. 39-48 (1960).

40. Semeria, R., "Quelques Resultats sur le Mechanisme de l'Ebullition," 7, J. de l'Hydraulique de la Soc. Hydrotechnique de France (1962).

41. Gaertner, R. F., "Photographic Study of Nucleate Pool Boiling on a Horizontal Surface," J. Heat Trans., 87, pp. 17-29 (1965).

42. Kirby, D. B. and Westwater, J. W., "Bubble and Vapor Behavior on a Heated Horizontal Plate During Pool Boiling Near Burnout," Chem. Engrg. Prog. Symp. Ser. 61, 57, pp. 238-248 (1965).

43. Danilova, G. N., "The Effect of the Number of Active Nuclei on the Rate of Heat Transfer in Large Volume Nucleate Boiling," NASA TT-F-11-305 (1967) from Inz. Fizicheskiy Zhy. XI, pp. 367-370 (1966).

44. Nishikawa, K., "Nucleate Boiling Heat Transfer of Water on the Horizontal Roughened Surface," Memoirs of Faculty of Enq. Kyushu Univ., 17, pp. 85-103 (1958).

45. Yamaqata, K., Hirano, F., Nishikawa, K. and Matsuoka, H., "Nucleate Boiling of Water on a Horizontal Surface," Mem. Fac. Engrg. Kyushu Univ., 15, 1, p. 97 (1955).

46. Nishikawa, K. and Yamagata, K., "On the Correlation of Nucleate Boiling Heat Transfer," Int. J. Heat Mass Trans., 1, p. 219 (1960).

47. Kurihara, H. M. and Myers, J. E., "Fundamental Factors Affecting Boiling," Amer. Inst. Chem. Engrgs. J., 6, p. 83 (1960).

48. Cornwell, K. and Borwn, R. D., "Boiling Surface Topography," 6th Heat Transfer Conference, Vol. 1, p. 157 (1978).

49. Heled, Y., Richlis, J. and Orell, A., "Pool Boiling from Large Arrays of Artificial Nucleation Sites," Int. J. Heat Mass Trans., 13, pp. 503-516 (1970).

50. Orell, A., "On S-Shaped Boiling Curves," Int. J. Heat Mass Trans., 10(7), pp. 967-971 (1967).

51. Tien, C. L., "A Hydrodynamic Model for Nucleate Pool Boiling," Int. J. Heat Mass Trans., 5, p. 533 (1962).

52. Zuber, N., "Nucleate Boiling. The Region of Isolated Bubbles and the Similarity with Natural Convection," Int. J. Heat Mass Trans., 6, pp. 53-78 (1963).

53. Bankoff, S. G., "On the Mechanism of Subcooled Nucleate Boiling - I. Preliminary Considerations," Chem. Engrg. Prog., Symp. Ser. No. 32, 57, p. 164 (1960).

54. Bankoff, S. G., "On the Mechanism of Subcooled Nucleate Boiling - II. Sequential Rate Process Model," Chem. Engrg. Prog. Symp. Ser. No. 32, 57, p. 164 (1960).

55. Zuber, N., "Hydrodynamic Aspects of Nucleate Pool Boiling, Part -I The Region of Isolated Bubbles," Rep. RQ-R1-164 (1960), AEC. Rep. T.I.D. 6338. Office Tech. Ser., Dept. of Com., Wash., D.C.

56. Ruchenstein, E., "Remarks on Nucleate Boiling Heat Transfer from a Horizontal Surface," Int. J. Heat Mass Trans., 9, 229 (1966).

57. Zuber, N., "The Dynamics of Vapor Bubbles in Nonuniform Temperature Fields," Int. J. Heat Mass Trans., Vol. 2, pp. 83-98 (1961).

58. Fritz, W., "Berechnung des Maximalvolumes von Dampfblasen, Phys. Z. 36, p. 379 (1935).

59. Hsu, Y. Y. and Graham, R. W., "An Analytical and Experimental Study of the Thermal Boundary Layers and Ebullition Cycle in Nucleate Boiling," NASA TND-594 (1961).

60. Han, C. Y. and Griffith, P., "The Mechanism of Heat Transfer in Nucleate Pool Boiling Part I, Bubble Initiation, Growth and Departure," Int. J. Heat Mass Trans., 8(6), pp. 887-904 (1965).

61. Shoukri, M. and Judd, R. L., "Nucleation Site Activation in Saturated Boiling," J. Heat Trans., Trans. ASME, 97, pp. 93-98 (1971).

62. Brown, W. T., "Study of Flow Surface Boiling," Ph.D. Thesis, Mech. Engrg. Dept., MIT (1967).

63. Bier, K., Gorenflo, D. and Wickenhauser, G., Bull. Inst. Int. Froid, Annexe, p. 63 (1971-2).

64. Bier, K., Gorenflo, D., Salem, M. and Tanes, Y., "Pool Boiling Heat Transfer and Size of Active Nucleation Centers for Horizontal Plates with Different Surface Roughness," 6th Int. Heat Transfer Conference, Vol. 1, pp. 151-156, Toronto (1980).

65. Gaertner, R. F., "Distribution of Active Sites in the Nucleate Boiling of Liquids," G.E. Report No. 61-RL-2826 C (1961).

66. Borishanskii, V., Bobrovich, G. and Minchenko, F., "Heat Transfer From a Tube to Water and to Ethanol in Nucleate Pool Boiling," in Symposium of Heat Transfer and Hydraulics in Two-phase Media, Edited by Kutateladze, S. S., Gosenergoizdat, Moscow (1961).

67. Cichelli, M. T. and Bonilla, C. F., "Heat Transfer to Boiling Under Pressure," Trans. Am. Inst. Chem. Engrgs. 41, pp. 775-787 (1945).

68. Borishanskii, V., Kozyrev. A. and Svetlova, L., eat Transfer in the Boiling of Water in a Wide Range of Saturation Pressure," High Temperature 2(1), pp. 119-121 (1964).

69. Magrini, U. and Nannei, E., "On the Influence of the Thickness and Thermal Properties of Heating Walls on the Heat Transfer Coefficients in Nucleate Pool Boiling," J. Heat Trans., 97 C, pp. 173-178 (1975).

70. Elrod, W., Clark, J., Lady, E. and Merte, H., "Boiling Heat Transfer Data at Low Heat Flux," J. Heat Trans., 87 O, pp. 235-243 (1967).

71. Chen, J. C., "Correlation for Boiling Heat Transfer to Saturated Fluids in Convective Flows " Ind. Eng. Chem. Process Design and Development, 5, p. 322 (1966).

72. Martinelli, R. C. and Nelson, D. B., "Prediction of Pressure Drop During Forced Circulation Boiling of Water," Trans. ASME, 70, p. 695 (1948).

73. Gunther, F. C., "Photographic Study of Surface-Boiling Heat Transfer With Forced Convection," Trans. ASME, 73, p. 115 (1951).

74. Thom, J. R. S., Walker, W. M., Fallon, T. A. and Reising, G. F. S., "Boiling in Subcooled Water During Flow Up Heated Tubes or Annulis," Symposium on Boiling Heat Transfer in Steam Generating Units and Heat Exchangers held in Manchester, Sept. 15-16, 1965 by Ins. of Mech. Engrs. (London).

75. Staniszewski, B. E., "Nucleate Boiling Bubble Growth and Departure," MIT Tech. Report No. 16, Division of Sponsored Research, Cambridge, MA (1959).

76. Nishikawa, K. and Urakawa, K., "An Experiment of Nucleate Boiling Under Reduced Pressure," Memoirs of Faculty of Eng., Kyushu Univ., 19(3), pp. 63-71 (1960).

77. Keshock, E. G. and Siegel, R., "Forces Acting on Bubbles in Nucleate Boiling Under Normal and Reduced Gravity Conditions," NASA TN-D-2299 (1964).

78. Hatton, A. P. and Hall, I. S., "Photographic Study of Boiling on Prepared Surfaces," Proc. 3rd Int. Heat Trans. Conf., Chicago, IV, pp. 24-37 (1966).

79. Cole, R. and Shulman, H. L., "Bubble Departure Diameters at Subatmospheric Pressures," Chem Eng. Prog. Symp. Ser. 62, pp. 6-16 (1966).

80. Van Stralen, S. J. D., "The Mechanism of Nucleate Boiling and in Binary Mixtures, Part I," Int. J. Heat Mass Trans., 9, pp. 995-1020 (1966).

81. Tolubinsky, V. I. and Ostrovsky, J. N., "On the Mechanism of Boiling Heat Transfer," Int. J. Heat Mass Trans., 9, pp. 1463-1470 (1966).

82. Beer, H., "Beitrag zur Wörmeubertragüng beim Sieden," Prog. Heat Mass Trans., 2, pp. 311-370 (1969).

83. Wang, A. C., Winter, E. R. F. and Mc Fadden, P. W., "The Relations Between Bubble Breakoff Diameter and Release Frequency in Nucleate Boiling of Liquid Nitrogen and Liquid Helium," Heat Transfer Laboratory, School of Mechanical Engineering, Purdue University, Lafayette, IN (1969).

84. Konig, A., "Uber den Einfluss der Heizwandeigenschaften ouf den Warmeubergang bei der Blasenverdampfung," Diss. D83, Berlin (1971).

85. Lindenstjerna, W. C. C., "Bubble Departure Diameter and Release Frequencies During Nucleate Pool Boiling of Water and Aqueous Sodium Chloride Solutions," in Heat Transfer in Boiling, Edited by Hahne, E. and Grigull, U., pp. 53075 (1977), Academic Press.

86. Kreshchev, G. G., "The Number of Vapor-Formation Centers in Surface Boiling," in Convective Heat Transfer in Two-Phase and One-Phase Flows, Edited by Borishanskii, V. M. and Pallev, I. I., Translated from Russian by the Isreal Program for Scientific Translations (1969).

87. Collier, J. G., Convective Boiling and Condensation, McGraw-Hill Book Company (UK) Limited (1972).

Distribution for NUREG/CR-2778 (ANL-82-32)

Internal:

E. S. Beckjord
C. E. Till
R. Avery
J. F. Marchaterre
A. J. Goldman
P. A. Lottes
L. W. Deitrich
D. Rose
D. H. Cho
P. B. Abramson
B. W. Spencer
W. A. Ragland
H. Komoriya
D. P. Weber
W. T. Sha
Y. W. Shin
D. M. France
W. L. Chen
T. C. Chawla
H. U. Wider
M. Ishii (20)
ANL Patent Dept.
ANL Contract File
ANL Libraries (2)
TIS Files (6)

External:

NRC Washington, for distribution per R2 and R4 (395)
DOE-TIC (2)
Manager, Chicago Operations Office, DOE
President, Argonne Universities Association
Reactor Analysis and Safety Division Review Committee:
W. P. Chernock, Combustion Engineering, Inc., 1000 Prospect Hill Road, Windsor, Conn. 06095
L. C. Hebel, Xerox Corp., 3333 Coyote Hill Road, Palo Alto, Calif. 94304
W. Kerr, The University of Michigan, Ann Arbor, Mich. 48105
S. Levine, NUS Corp., 4 Research Place, Rockville, Md. 20850
S. Levy, S. Levy, Inc., 1901 S. Bascom Ave., Campbell, Calif. 95008
T. H. Pigford, University of California, Berkeley, Calif. 94720
J. J. Taylor, Electric Power Research Inst., P. O. Box 10412, Palo Alto, Calif. 94303